

Review

Carbonaceous Materials as Anodes for Lithium-Ion and Sodium-Ion Batteries

Koorosh Nikgoftar ¹, Anil Kumar Madikere Raghunatha Reddy ¹, Mogalahalli Venkatashamy Reddy ² and Karim Zaghib ^{1,*}

¹ Department of Chemical and Materials Engineering, Concordia University, 1455 De Maisonneuve Blvd. West, Montreal, QC H3G 1M8, Canada; koorosh.nikgoftar@mail.concordia.ca (K.N.); anil.mr@concordia.ca (A.K.M.R.R.)

² Nouveau Monde Graphite (NMG), Saint-Michel-des-Saints, QC J0K 3B0, Canada; reddymvvr@gmail.com

* Correspondence: karim.zaghib@concordia.ca

Abstract: The increasing global population and, thus, energy demand have made research into renewable energy sources more critical. Lithium-ion batteries (LIBs) and sodium-ion batteries (SIBs) have been recognized as the most promising technologies for storing energy and effectively addressing this demand. Carbonaceous materials are the most widespread anode material due to their fascinating features, such as high theoretical capacity, high electrical conductivity, and excellent structural stability. Additionally, these materials' abundance, cost-effectiveness, and environmental friendliness have emphasized the need for further investigation and development. Among these carbon-based materials, graphite (both artificial and natural) stands out as the most ubiquitous anode material due to its layered crystal structure, high mechanical strength, long cycle life, and excellent safety profile, making it ideal for intercalation with lithium and sodium. In recent years, extensive research has been conducted to enhance the efficiency of anodes and, ultimately, the overall performance of batteries. In this review, the role of carbonaceous materials in anodes for lithium-ion and sodium-ion batteries was comprehensively investigated, focusing on advancements in synthesizing and optimizing artificial graphite. Furthermore, the intercalation mechanism and the factors influencing the electrochemical properties of both LIBs and SIBs were extensively discussed. This work also provides a holistic perspective on the differences between these two types of batteries, highlighting their cost, safety applications, and future potential advancement.



Academic Editor: Yong-Joon Park

Received: 25 February 2025

Revised: 18 March 2025

Accepted: 19 March 2025

Published: 25 March 2025

Citation: Nikgoftar, K.; Madikere Raghunatha Reddy, A.K.; Reddy, M.V.; Zaghib, K. Carbonaceous Materials as Anodes for Lithium-Ion and Sodium-Ion Batteries. *Batteries* **2025**, *11*, 123. <https://doi.org/10.3390/batteries11040123>

Copyright: © 2025 by the authors. Licensee MDPI, Basel, Switzerland. This article is an open access article distributed under the terms and conditions of the Creative Commons Attribution (CC BY) license (<https://creativecommons.org/licenses/by/4.0/>).

1. Introduction

The increasing world population and the diminishing amount of fossil fuels highlight the need to find renewable energy sources. Fossil fuels also have an irreversible impact on nature and our lives. In the past, researchers explored promising alternative renewable energy sources such as wind, solar, and hydropower. None of the mentioned sources are entirely reliable or feasible for consistent, long-term use [1]. Rechargeable batteries are a potent solution for storing energy and powering electronic devices and vehicles. They can eventually alleviate the environmental impact of fossil fuels and reduce the carbon footprint. There are various types of batteries, but lithium-ion batteries (LIBs) and sodium-ion batteries (SIBs) stand out as the top performers in various applications and sectors [2–6]. Recently, these batteries have become ubiquitous and have gained researchers' interest. LIBs

are highly valued for their energy density, durability, and eco-friendliness [7,8]. Likewise, SIBs are valued for their abundant raw materials and lower cost, which make them a promising alternative [9]. The primary model of these batteries constitutes a cathode made of lithium or sodium complexes and carbonaceous materials that can be perfectly implemented as an anode. A porous separator serves as a barrier between these two parts to prevent a short circuit, and the cell is filled with an electrolyte composed of an organic or inorganic solvent and an accompanying proper metal salt [10,11]. The main concept of these batteries involves the transport of ions and electrons from the cathode to the anode, where ions intercalate into the anode material during charging [12].

1.1. Anode Materials and Costs

One of the crucial components of the batteries is the anode, which has physical and chemical properties that significantly influence the efficiency and performance of the battery. Anode materials should be capable of accepting lithium and sodium ions. The amount of these ions must be maximized to achieve the highest battery capacity. Additionally, it is worth noting that the structure of the anode must not undergo structural damage and exfoliation during the charge/discharge cycle [13]. Carbon-based materials have, indeed, become increasingly popular in the field of battery technology due to their low cost, high electrical conductivity, and excellent stability. These materials are being extensively researched as electrode materials for various batteries, leveraging their resource abundance and non-toxicity [14–19]. These anode materials are mainly categorized into graphite, soft carbon, hard carbon, graphene, carbon nanotubes (CNTs), alloys, etc. (Figure 1a) [20–22]. The preparation conditions of these materials significantly impact their structural arrangement, resulting in different carbon forms and hybridization, and their final cost (Figure 1b) [23,24]. Due to its excellent performance characteristics, natural graphite (NG) is the cheapest and primary anode material for LIBs. Having said that, due to the larger size of sodium, which leads to thermodynamic instability, graphite may experience exfoliation and limited electrochemical intercalation; hard carbon, instead, performs better in these batteries [25].

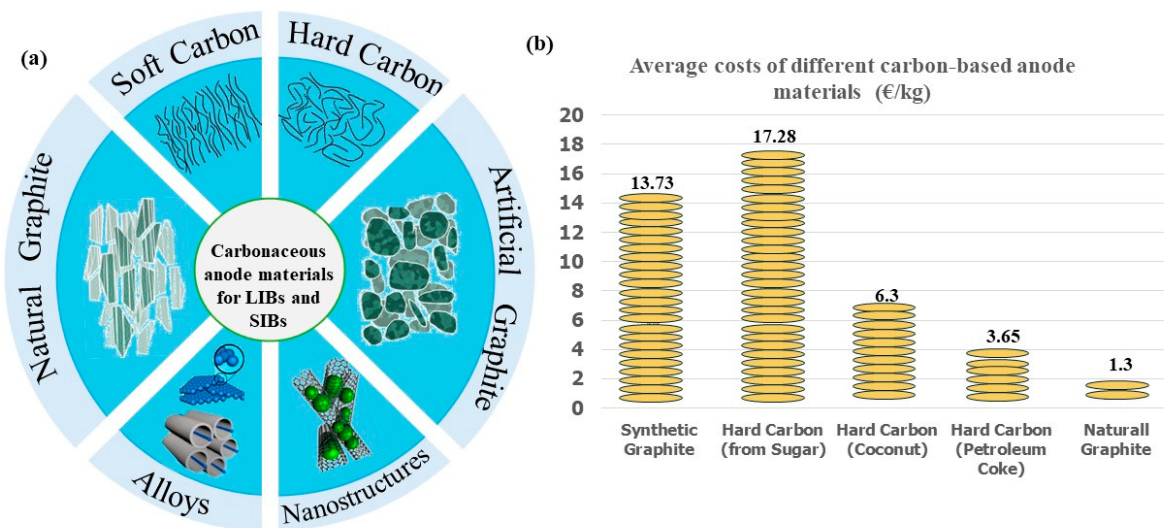


Figure 1. (a) Carbonaceous anode materials for LIBs and SIBs [26,27]. (b) Comparative cost analysis of anode materials for lithium-ion (LIBs) and sodium-ion batteries (SIBs).

The cost of LIBs and SIBs highly depends on the type of anode material, type of application, and manufacturing process. As the most ubiquitous anode material, NG in anodes is cost-effective due to abundant raw materials and being bulk-mined. It is widely used in EVs and portable electronic devices, for which stability and affordability are a

priority. A hard carbon anode is used for fast-charging devices due to its high capacity and fast-charging capacity [28]. This anode type is more expensive, requiring additional processing steps such as high-temperature treatment. Advanced materials such as silicon–carbon composites promise better energy density but are still expensive due to complicated synthesis [29]. Regarding the overall cell cost, Petera et al. estimated the cost of an 18650-type SIB cell to be 223 EUR/kWh, and LIBs have varying costs based on their cathodes. Lithium–iron–phosphate (LFP) cells were priced at 229 EUR/kWh, whereas lithium–nickel–manganese–cobalt (NMC) cells were lower at 168 EUR/kWh. The anode component does not largely influence the cost of LIBs and SIBs. In SIBs, the anode makes up just 17.9% of the total cost, while for LIBs, it accounts for only 15.6% [30,31].

1.2. Hard Carbon and Soft Carbon

Amorphous carbon has demonstrated exceptionally remarkable performance in SIBs. This material is mainly categorized into soft carbon (SC) and hard carbon (HC) based on how hard it is for them to be converted into graphite [32]. The prominent differences between these materials are their structural properties and the application types used. HCs have a disordered microstructure with extensive small pores and a high specific surface area [33], and it is difficult to prepare high-crystallinity synthetic graphite, even at higher temperatures (greater than 3000 °C) [34]. There are several alternative methods for preparing hard carbons, the most common of which is the pyrolysis of precursors. This process involves the thermal decomposition of carbon-rich materials such as polymers [35], biomass (plant-based materials) [36], and pitches [37]. HCs are considered the most sustainable anode materials for sodium storage due to their larger interlayer spacing compared to NG (40 nm versus 33 nm) [38], which facilitates sodium storage. These anode materials maintain high capacity and a negative potential range, even under substantial current densities. Additionally, their high degree of disorder and numerous defect sites contribute to increased electrochemical activity and an active surface area. Having said that, the higher surface area of the anode in SIBs lowers the initial Coulombic efficiency (ICE) due to increased sodium ion adsorption, resulting in excessive solid electrolyte interphase (SEI) formation and irreversible sodium consumption. Several modifications have been implemented to address this limitation; Ren et al. significantly improved the ICE of HCs by doping them with chlorine, which decreases the formation of the SEI film by tuning the electronic structure [39]. Another optimization strategy for improving ICE is the carbonization process. This method involves temperature control to minimize defect size and decrease surface area, followed by a two-step carbonization process. This step begins by heating the material at a lower temperature to promote the formation of a more ordered structure, and the second step uses a higher temperature to graphitize the material further. This strategy reduces structural defects, leading to an increase in ICE [40,41]. Another significant drawback is the formation of sodium dendrites, which arise from the association of hard carbon occurring below 0.2 V vs. Na^+/Na , resulting in a plateau in the potential graph; however, this can be alleviated by the mentioned strategies [42,43].

SCs have short microcrystalline structures that are arranged such that they can be transited to graphite at high temperatures (2800 °C), forming a graphite-like structure. This structure improves the ionic conductivity and rate capacity compared to the convoluted structure of HCs [44]. SCs are frequently utilized in hybrid systems for high-voltage supercapacitors due to their superior charge/discharge efficiency and capacity to form additional pathways [33]. However, SCs suffer from a low initial capacity compared to HCs, and several research studies have been carried out regarding this matter, such as hetero-atom doping to enhance electrochemical performance [45,46], conductive material coating, and creating a composite with other high-capacity materials [47].

2. Graphite

Graphite is the most ubiquitous anode material for LIBs (surpassing amorphous carbon) due to its exceptional performance. Since the early 1990s, when the Sony Corporation commercialized LIBs, graphite consumption has increased. By 2010, the global consumption of graphite was 1.1 million tons. With the significant rise in demand for EVs (electronic vehicles), this trend has continued, driven by increasing demand from the battery sector. By 2023, global annual graphite consumption had surged to almost 4.6 million tons. A summary of the leading graphite-mining countries over the last five years is presented in Table 1. It is also worth mentioning that, over the previous five years, most of the published papers regarding anode materials for both LIBs and SIBs were related to graphite (Figure 2a,b) [48–51].

Table 1. Leading countries for graphite mining over the last five years (in 1000s of metric tons) [52].

	2023	2022	2021	2020	2019
China	1300	1000	820	820	780
Mozambique	96	166	77	120	150
Brazil	73	73	82	92	90
Canada	3.5	13	42	40	35
India	11.5	11	10	10	39
South Korea	27	24	11		
Russia	16	16	16	16	16
Norway	10	7	12	10	10

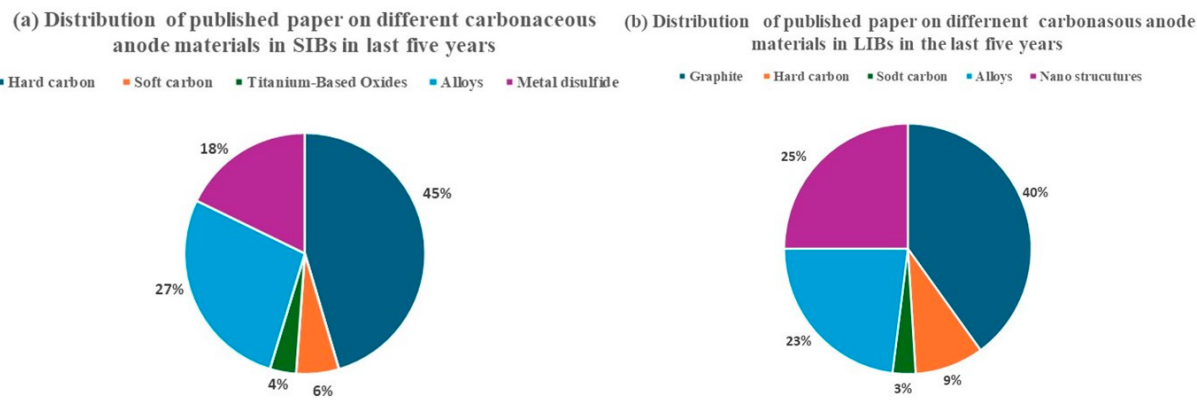


Figure 2. Distribution of published papers on various carbonaceous anode materials for (a) SIBs and (b) LIBs based on data collected from Web of Science.

Graphite offers a high theoretical specific capacity of 372 mAh g^{-1} , with a plateau at low potential ($0.1 \text{ V vs. Li}^+/\text{Li}$), which maximizes the final battery voltage [53–55]. Furthermore, graphite's ICE is higher than amorphous carbon, as a thinner SEI layer forms on the electrode [56]. Graphite has a highly crystalline and hexagonal layered structure that is held together by van der Waals forces [36]. These layers are mainly stacked in ABAB (Bernal stacking) or ABC (rhombohedral stacking) forms. This arrangement results from the $\pi-\pi$ interactions between Sp^2 carbon atoms [57]. The electronic properties of graphite are highly dependent on its stacking structure, with ABC-stacked graphite exhibiting superior performance in terms of electrical conductivity, charge carrier mobility, and interlayer interactions compared to other stacking configurations [58].

2.1. Graphite Intercalation Compounds

Graphite intercalation compounds (GICs) form when atomic or molecular layers intercalate (i.e., are placed between) their host, which is graphite. These compounds

feature high structural order and differ based on their staging phenomena [25]. These phenomena occur during intercalation, forming a unique phase in the anode that impacts the performance of batteries. The stage order is assigned by “n”, which is the number of graphite layers between the two nearest intercalate layers.

The aromatic rings in graphite conjugate over the structure, resulting in the delocalization of π electrons above and below the plane of atoms, making the ring suitable for accepting or losing electrons. An alkali metal ion, such as a lithium ion, donates an electron to the π orbital, and an increase in ion concentration leads to increasing Coulombic repulsion, which can cause a defect in the binding force between the graphite layer and form stable GICs. Equation (1) reveals the intercalation mechanism in graphite [59,60]:



Based on the preparation process, graphite is categorized as natural graphite (NG) or artificial graphite (AG) [61]. The most popular NG is flake graphite, which is initiated from deposits and undergoes mining and purification processes to qualify as an anode material [62] that, when compared to AG, requires lower costs and less energy [63]. Having said that, flake graphite prepared under extreme conditions has large anisotropy and extensive structural defects, which have an impact on its sustainability during the charge/discharge cycle and may also result in extensive SEI formation and exfoliation [64]. Several modifications have been made to avoid this exfoliation and increase the cycle life of flake graphite. Surface modifications such as carbon coating [65–67], catalytic modification [68], high-shear exfoliation, and temperature control treatment have been revealed to be effective in improving the cycle life of NG [69].

2.2. Artificial Graphite

2.2.1. Synthesis

Artificial graphite (AG), also called synthetic graphite, is one of the most famous anode materials for battery applications. In 2023, around 70% of lithium-ion battery anodes were composed of AG, with manufacturing dominated by Chinese factories. The invention of AG by Acheson dates back to 1898, when pure graphite was produced by overheating silicon carbide (SiC_2), a highly crystalline compound [70,71]. Since then, the Acheson method has been utilized to convert carbon-rich substances, such as meso-carbon microbead (MCMB) [58], petroleum precursor [59], needle coke, and pitch, by applying high temperatures (around $2800\text{ }^\circ C$) for extended periods [72]. Hwang et al. prepared AG using different-sized needle coke, which was crushed, mixed with a binder, and then molded at a high temperature. This step was first followed by carbonization at $900\text{ }^\circ C$ (N_2 atmosphere) and graphitized at $2700\text{ }^\circ C$ (He atmosphere) to boost crystallinity and electrochemical performance (Figure 3) [73].

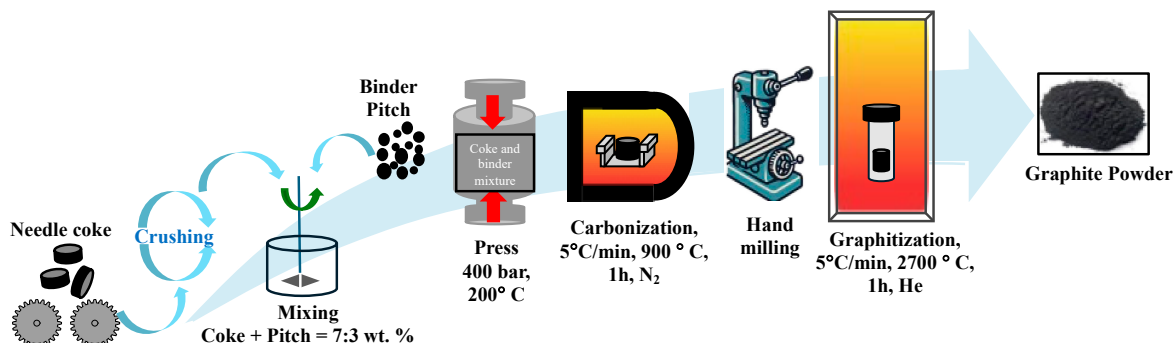


Figure 3. Synthesis of AG via the graphitization process using needle coke as the precursor [73].

Several other methods have been implemented to minimize energy consumption and reduce the final cost. The catalytic reaction is one modification that can lower the temperature required for a graphitizing reaction; however, the purity of the final product drops significantly [74,75]. Electrochemical graphitization is another efficient recently developed method that can be used for various types of amorphous carbon, even for non-graphitizable types. In this process, raw materials undergo a phase transformation process, which results in cathodic polarization in molten CaCl_2 at around 820°C (1100 K). The final product is graphite nanosheets with high purity and crystallinity [76]. Table 2 provides alternative methods to prepare AG and the electrochemical properties of the final anode. High-temperature graphitization, which can be applied to various types of carbon-based compounds, can produce the most crystalline and high-performance AG; this makes it ideal for applications that require long cycle life while having a great capacity [77]. Catalytic and electrochemical graphitization reactions enhance cost-effectiveness by lowering the required temperature. In addition to being a more sustainable and economical alternative, they optimize anode performance and specific capacity while improving ion diffusion and charge transfer kinetics, making them ideal for fast-charging anode applications.

Table 2. Comparison of AG synthesis methods and their electrochemical performance.

Method	Graphitization Temp ($^\circ\text{C}$)	Voltage Range (V)	Specific Capacity ($\text{mA}\text{h}\text{g}^{-1}$)	Cycle Life	ICE	Ref.
Graphitization of needle coke	2700	0.05–1.3	~325 at 0.1 C	98.7% after 100 cycles at 0.1 C	>90%	[73]
Graphitization of bituminous coal	2000–2800	0.001–2.0	310 at 0.1 C	95.3% retention after 100 cycles at 0.1 C	~87%	[78]
Graphitization of anthracite coupled with effective catalyst (boron oxide)	2700	0.001–2.0	~320 at 0.5 C	98% after 500 cycles at 0.5 C	~81%	[79]
Catalytic graphitization	2600	0.001–2.0	372 at 0.2 C	89.2% after 500 cycles at 2 C	85.88%	[80]
Low-temperature electrochemical graphitization of biomass-derived activated carbon from coconut waste in molten salts	850	0.01–3.00	282 at 1 C–200 at 5 C	92% after 1000 cycles at 5 C	~65%	[81]
Graphitization of CO_2 -derived carbon	2800	0.01–2.0	297–378.1 at 50 mAg^{-1}	~100% after 300 cycles at 1 Ag^{-1}	72.6–80.5%	[82]

2.2.2. Doping Carbon Materials

Several modifications have been implemented to increase the efficiency of graphite, including morphology control and nanostructure engineering [83], layer and porosity engineering and surface modifications to increase reaction kinetics [84], and pore structure design [85]. Among these, doping has been widely recognized as an effective strategy to enhance electrochemical performance. Introducing an element or complex in the lattice of graphite without altering its structure and changing its charge and spin distribution is a doping modification. Hetero-atoms (N, O, S, P, Cl, Br, and I) are the most famous dopants that have an impact on interlayer spacing, anode defects, electrical conductivity, ion diffusion rate, and the activity of anode materials, i.e., they increase the efficiency of SIBs or LIBs [86,87]. Nitrogen and sulfur doping are the most studied methods, which increase carbon's reactivity and electronic conductivity by creating auxiliary defects and expanding carbon layer spacing [88,89]. The specific capacity of nitrogen and sulfur dual-doped graphite rises to

1460 mAhg^{-1} at 0.25 C [90]. This modification is favorable for high-power applications and SIBs to accommodate large sodium ions; however, this doping method decreases the surface area and lowers the ICE [91]. Nitrogen can be doped in the graphite layer in three forms: pyridinic, pyrrolic, and graphitic. Sulfur can form dipole or carbon–sulfur bonds due to its larger size (larger than nitrogen), and it has a greater impact on increasing interlayer spacing than nitrogen [91,92]. Phosphorus is another hetero-atom dopant, which increases the defects and surface area to achieve lower electronegativity than carbon and decreases the energy gap between the valence band and the conduction band [93]. This method significantly improves the electrochemical performance of anode materials; however, due to phosphorus's larger atomic radius and high binding energy, the doping process is complex and requires extensive effort. The specific capacity of phosphorus-doped carbon balls with 4% phosphorus in SIBs can reach 340 mAhg^{-1} at 1 Ag^{-1} , which is approximately four times higher than that of commercialized graphite anode (less than 100 mAhg^{-1} in the same conditions) [94]. Similarly, surface fluorination increases surface area by reducing oxygen-containing surface groups, leading to greater surface disorder [95].

2.3. Comparative Analysis of Natural and Artificial Graphite

AG and NG are both widely used as anodes in LIBs. They provide distinct features that influence the overall performance of the application.

2.3.1. Structural Analysis

Artificial graphite has an ABA stacking structure with turbostratic disorder (Figure 4a), high crystallinity, and a more compact structure with no voids inside, enabling it to have higher electrode density, rate capacity, and stability than NG [61,73]. This highly ordered structure makes AG a desirable anode material for applications requiring a long cycle life and a low self-discharge rate. Having said that, the reduced defect sites in AG can decrease ion diffusion rates and lower the overall C rate of the battery. This can be a significant drawback for fast charging. For instance, in EVs where the main focus is on how fast the car is charged, AG may not always be the optimal choice despite its stability and durability. The lower surface area minimizes side reactions and prevents the formation of a thick SEI layer, reducing internal resistance and increasing battery efficiency [96,97].

In contrast, NG has less ordered structures with defects and a higher porosity degree, which can be found in the two stacking forms of ABA and ABC (Figure 4a). These features lead to increased surface area, greater capacity, quicker ion diffusion, and thicker SEI layer formation, which are ideal for the majority of applications (Figure 4b) [98].

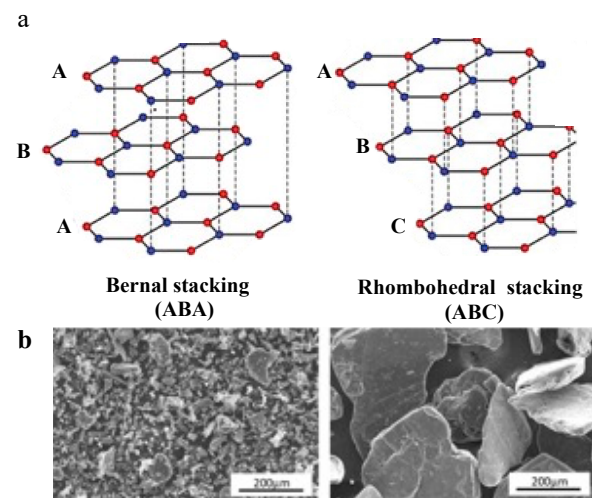


Figure 4. (a) Stacking structure comparison of NG and AG. (b) Scanning electron microscope (SEM) image of NG and AG [99,100].

2.3.2. Electrochemical Behavior

The electrochemical properties of natural graphite (NG) and artificial graphite (AG) anode may exhibit both similarities and differences, influencing their potential for commercial applications. (Figure 5a) depicts the charge/discharge curves of both AG and NG anodes in LIBs. The initial reversible capacity of both anodes is almost the same, with a slightly higher value for NG (360.4 mAhg^{-1}) compared to AG (355.5 mAhg^{-1}). This indicates that NG has a greater intercalation capacity and lithium storage capability and higher energy density. Despite these facts, NG suffers from a lower ICE than AG (93.13% compared to 94.07% for AG), reinforcing the fact that NG experiences higher initial capacity loss and forms a more robust SEI layer. It can be comprehended from Figure 5b that NG possesses a stronger cathodic and anodic peak than AG, reflecting a faster ion diffusion rate and improved ion intercalation reversibility. Additionally, NG exhibits less polarization than AG, resulting in superior rate capability and making it ideal for applications requiring high power output. Figure 5c illustrates that NG experienced faster capacity fading than AG due to higher ion consumption, but its performance stabilizes over further cycles. AG has better initial stability, but it experiences greater resistance growth over time, leading to have similar capacity for both anodes after 800 cycles [101].

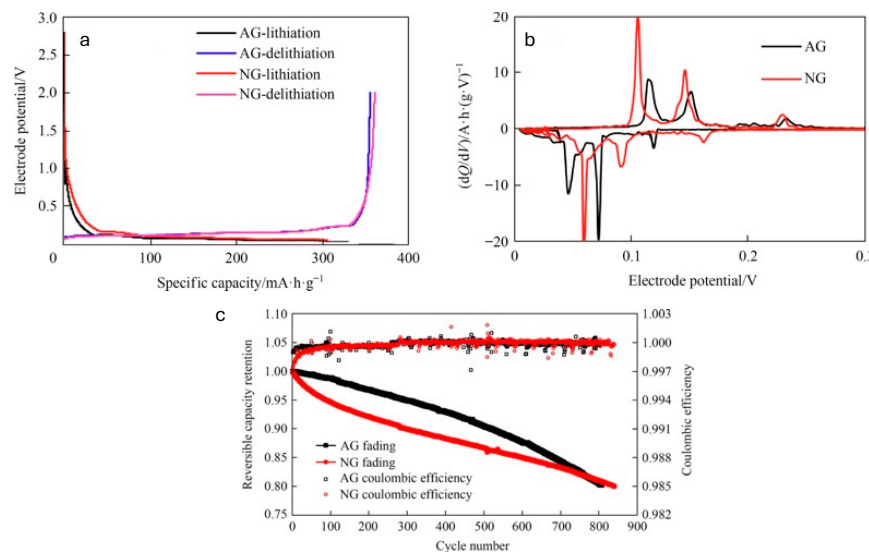


Figure 5. Electrochemical performance of artificial graphite and natural graphite anode.

One of the most prominent advantages of NG over AG is intercalation degradation. Figure 6 depicts the electrochemical behavior of AG and NG in LIBs containing ionic liquid electrolytes. The graphs show that AG peaks at around 1 V vs. Li/Li⁺, indicating undesired cation intercalation, which results in structural degradation after intercalation. On the other hand, NG can form better metal-ion intercalation and better long-term performance [102]. The process required for mining NG involves lower energy consumption and expenses than AG. It is also more abundant; therefore, it is more cost-effective, which makes it more widely suitable. It is worth mentioning that, owing to more defect sites, NG metal contamination is higher than AG; therefore, restoring and recycling NG costs more and produces more environmental concerns [103]. On the other hand, AG is more costly because the manufacturing process requires high-energy and high-temperature processes to achieve the required crystallinity and purity.

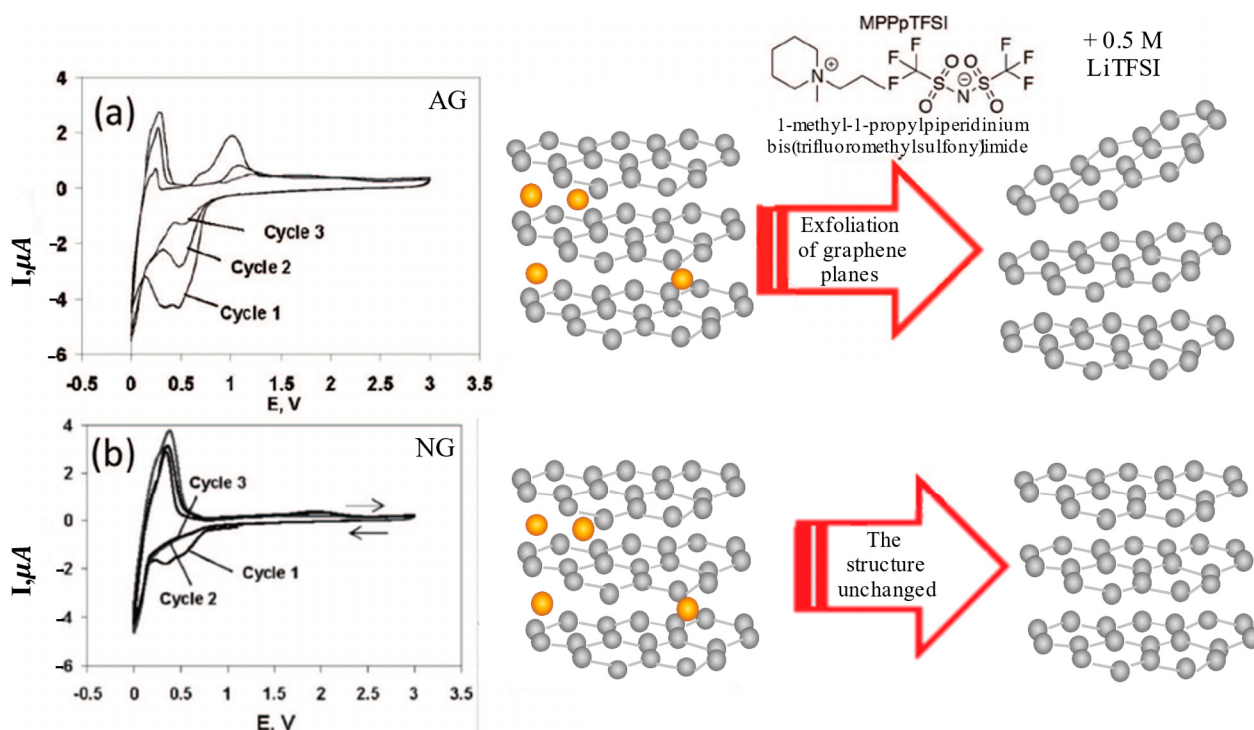


Figure 6. AG and NG intercalate. **(a)** Synthetic graphite; IL cation intercalation occurs with Li-ion intercalation. **(b)** For NG, electrode surface passivation occurs with Li-ion intercalation, resulting in Li^+ desolvation without co-intercalation of the IL cations.

Sustainability and economic factors also play a crucial role in material selection. The process required for mining NG involves lower energy consumption and expenses than AG. It is also more abundant, making it a more cost-effective and widely available option. Owing to more defect sites, NG metal contamination is higher than AG; therefore, restoring and recycling NG costs more and has more environmental concerns. On the other hand, AG is more costly as the manufacturing process takes high energy and requires high-temperature processes to achieve the required crystallinity and purity. As industries move towards batteries with a lower environmental footprint, the environmental impact of AG production has raised concerns, promoting research and studies into lower-energy synthetic graphite alternatives and more efficient NG purification methods. Despite these facts, AG has a more stable structure, is a safer choice, and has a longer cycle life, making it perfect for EVs. Meanwhile, NG remains a strong alternative for lower-cost, high-energy-density applications, especially where sustainability and raw material availability are priorities [104].

2.4. Electrochemical Properties vs. Forms of Carbon

The primary structure of AG is highly dependent on its carbon precursor and the graphitization procedure. The final structure greatly impacts the electrochemical properties of the anode materials. Xing et al. presented five types of AG, each prepared under distinct conditions and graphitization temperatures, and conducted a comprehensive analysis of their electrochemical properties as electrodes. The result clearly elucidated that the spacing layer distance does not differ significantly with increasing the temperature. However, the graphitization temperature strongly influences the microstructure of the materials; higher temperatures (up to 2800 °C) result in a more ordered layered structure, a higher graphitization degree, and well-developed mesopores. These structural improvements enhance electrochemical performance, providing favorable pathways for lithium-ion intercalation

and deintercalation; this leads to increased reversible capacity, superior rate capability, and excellent cycling stability [78,105].

Liu et al. studied AG for LIBs, examining how the primary precursor's crystal structure and electronic properties affect lithium storage performance. This study found that graphite with longer crystal planes and fewer stacking layers exhibits higher electron conductivity. Graphite with longer planes and fewer layers shows higher specific capacity at slow charge/discharge rates, while shorter planes and more layers perform better at rapid rates [106]. Herrin prepared a table (Table 3) summarizing the advantages, disadvantages, and key electrochemical properties of AG based on different precursors.

Table 3. Characterization of AG synthesized from different precursors.

Carbon Precursor	Advantages	Disadvantages	Reversible Capacity (mAhg ⁻¹)	Cycling Stability	Price (USD/kg)	Reference
Needle coke (10–15 µm)	High crystallinity, excellent structural stability, highly layered	High cost, limited pathways, lower rate capability	360–370 at 0.1 Ag ⁻¹	92.6% after 100 cycles	15–30	[73]
Needle coke (2–5 µm)	Short ion diffusion distance, high charge/discharge capability	Low volumetric density, high porosity	380–400 at 0.1 Ag ⁻¹	98.7% after 100 cycles	15–30	[73]
Porous activated carbon (PAC) from petroleum coke	Good graphitization potential, cost-effective, high surface area, great stability	Lower conductivity compared to needle coke	330–350 at 0.1 Ag ⁻¹	~98% after 15,000 cycles	-	[107]
Coal tar pitch	High graphitization potential	Impurities require removal	330–360 at 0.3 Ag ⁻¹	~95% after 100 cycles	10–20	[108]
Amorphous carbon (graphite derived from CO ₂ via LiAlH ₄ reaction)	Abundant, low cost, environmentally friendly, high purity	Poor conductivity, requires controlled pressure conditions	320 after 1500 cycles at 1 Ag ⁻¹	99% retention after 100 cycles	-	[109]
Biomass-derived carbon	Eco-friendly, renewable	Low graphitization degree	150–200 at 0.3 Ag ⁻¹	~90% after 150 cycles	10–20	[110]

3. Lithium-Ion Batteries

3.1. Intercalation

The invention of lithium-ion batteries is considered the cornerstone of modern energy storage technology. LIBs are used in portable electronic devices, electric vehicles (EVs), and renewable energy storage systems. These batteries are renowned for their exceptional energy density, long cycle life, and relatively low self-discharge rate [111–113]. Since their commercialization, extensive research and development have been undertaken focusing on enhancing the efficiency of these batteries. As a result, conventional LIBs achieve ~300 Wh/kg energy density, which is almost three times higher than the primary model [114,115]. This combination of features becomes more prominent in high-power devices such as EVs, where LIBs are considered the most promising power source for these vehicles. As a result of the growing tendency of these vehicles, the demand for LIBs has more than doubled from 330 GWh to 750 GWh over the past two years [116].

The mechanism of intercalation is still under debate. Several research studies have proposed different mechanisms, but none have been able to determine the proper intercalation dynamics confidently. In 1938, Rüdorff and Hofmann revealed that lithium could be inserted into a graphite lattice [117]. They noticed this phenomenon by observing X-ray diffraction and measuring the stepwise potential changes occurring during different stages (e.g., $n = 1$, $n = 2$), with each stage having a specific lithium content [118,119]. Their proposed model suggests that lithium ions are accommodated between the intermediate

layers of each carbon layer during the insertion process. However, similar to several other proposed models, there is controversy surrounding this method, as it does not account for the phase transition capability happening during intercalation [120]. After around 30 years, Daumas and Hérolé presented their model, where the conversion of stages occurs through rearranging the intercalant inside the lattice without altering whole layers. In this model, carbon monoxide prepares a new crystallographic phase when lithium ions are inserted in graphite, preventing the movement of the alkaline metal ions between the layers of graphite [121]. Ultimately, in 2013, by analyzing the dynamic lithium intercalation process *in situ*, He et al. determined that, at high energy density, the classical stage mechanism does not apply due to the polarization effect. They found a new approach in which this mechanism consists of several continuous steps, depending on the lithium content in the graphite. As the lithium concentration increases in the graphite lattice, meaning that higher-order compounds convert to a lower order, the voltage plateau decreases until graphite becomes completely saturated (LiC_6) (Figure 7) [86].

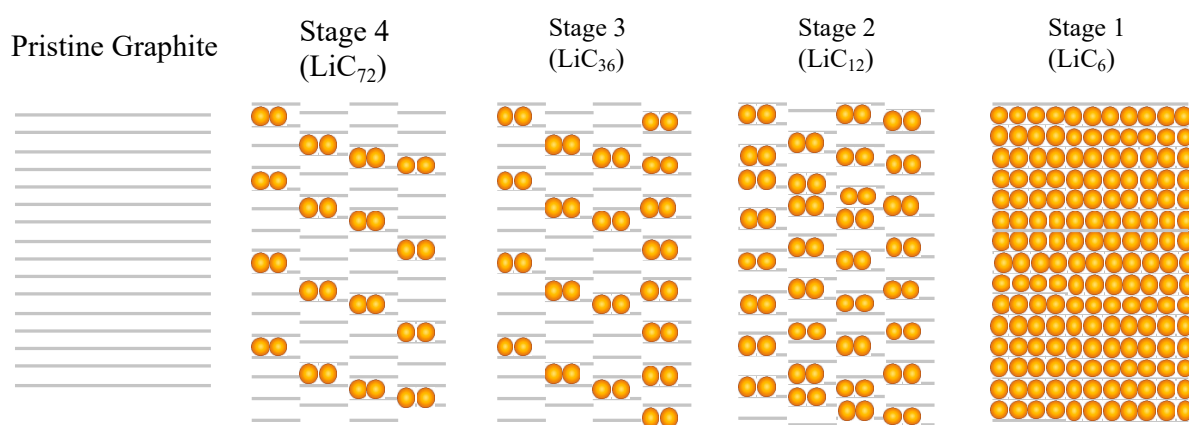


Figure 7. Graphite intercalation mechanism steps.

3.2. Cycle Life and Calendar Life

Primary lithium-ion batteries have fascinating features; however, they face degradation over time in terms of both cycle life and calendar life. It is estimated that, for stationary LIBs and EV batteries, 3500 and 1000 cycles, respectively, should be maintained to ensure long-term durability and optimal performance throughout the lifespan of the batteries [122]. Afterward, several research studies were conducted to increase these features, leading Tesla to introduce Model 3, which is equipped with lithium iron phosphate (LFP) batteries; these typically offer a cycle life of approximately 1500 cycles. Several factors are involved in their degradation process, including temperature, the state of charge (SOC), and the loss of secondary and primary materials [123].

High temperature can affect the battery's cycle life in various ways, including elevating the degradation of the SEI and the primary materials. It is worth pointing out that elevated temperature can temporarily decrease resistance; however, after multiple cycles, it leads to degradation, such as having a thicker SEI or the growth of lithium dendrites. This can eventually impair battery cycle and calendar life, especially when combined with high SOC levels [124,125]. A primary equation of how this resistance is related to temperature and SOC was provided by Wright et al.:

$$R(t, T, \text{SOC}) = a(\text{SOC})\exp\left[\frac{b(\text{SOC})}{T}\right]t^{\frac{1}{2}} + C(\text{SOC})\exp\left[\frac{d(\text{SOC})}{T}\right] \quad (2)$$

Equation (2) clearly states how resistance, temperatures, SOC, and diffusion-controlled processes evolve over time. This can help to understand the impact of temperatures on

both calendar life and cycle life by identifying the battery aging mechanism under various conditions [126]. It can also be concluded that these factors are dependent on the primary anode and cathode materials; as AG has a more porous structure, it will experience less temperature-induced degradation, reducing the growth of resistance. Furthermore, as there is a $t^{\frac{1}{2}}$ factor in the prepared model (Equation (2)) related to the diffusion-controlled processes, such as SEI growth, this suggests that a more stable SEI can be formed on AG, which leads to minimizing resistance increase and improving calendar and cycle life [127]. Table 4 depicts the retention rate after defined cycles for different worldwide types of anode materials.

Table 4. Retention capacity rates of different anode materials in lithium-ion batteries at 1 C at RT [128–133].

Anode Material	Retention Capacity Rate	Number of Cycles
Natural graphite	80–90%	500
Artificial graphite	95–98%	200
Graphite powder	94–96%	100
Carbon nanotubes	94.6%	50
Silicon–graphene	92.7%	50
Pre-lithiated hard carbon (PHC)	80%	300

Several strategies are available to improve the stability of SEI and the cycle and calendar life of graphite anode materials, including adding liquid additives to organic electrolytes. Vinylene carbonate (VC) is the most common among these additives, as it has a relatively low reduction activation energy (13 kcal/mol) and a high reduction potential (1.05–1.4 V Li/Li⁺) compared to other solvents such as ethylene carbonate (EC) and propylene carbonate (PC); these have higher activation energies (24.9 kcal/mol and 26.4 kcal/mol, respectively) and lower reduction potentials (0.65–0.9 V for EC and 0.5–0.75 V for PC). These features help to form a more stable SEI layer, reducing the degradation of anode materials and improving overall battery performance [134,135].

Another factor that significantly impacts battery cycle and calendar life is growing lithium dendrites, which can cause short circuits, capacity loss, and reduced efficiency [136]. Lithium salt electrolytes surrounded by solvent molecules and anions in electrolytes form a solvation shell. This shell influences lithium-ion diffusion, facilitates desolvation, and ensures controlled deposition on the anode [137]. External additives can weaken the solvent–ion interaction, leading to the formation of more contact ion pairs (CIPs) or ion aggregates (AGGs), which can minimize the energy for transporting lithium ions (Figure 8). This would result in a robust SEI, increased lithium diffusion, and regulated deposition on the anode, eventually decreasing the risk of lithium dendrites [138].

Reducing particle size also improves lithium-ion diffusion and transport kinetics, which enable batteries to have a faster charge/discharge rate and increase cycle stability. Composition strategies have been found to optimize both calendar and cycle life. Combining carbon-based materials with silicon or metal oxide can result in the benefits of nanoscale diffusion kinetics with the higher stability of larger particles, which results in a balance between the two features for the battery [139–141].

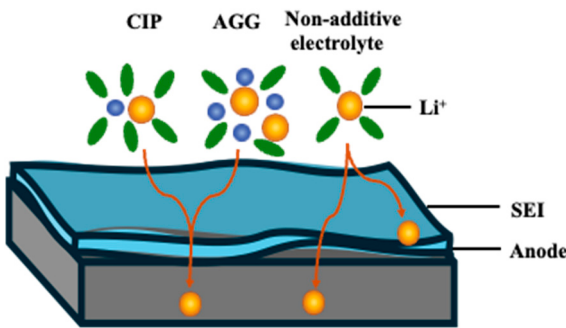


Figure 8. Enhanced lithium-ion diffusion facilitated by electrolyte additives compared to non-additive electrolytes.

3.3. Energy Density and Capacity

Before the advent of lithium-ion batteries (LIBs), the most prominent energy storage applications relied on lead–acid and nickel–cadmium batteries, as used in several industries, such as automotive and portable electronic devices. Those old-model batteries featured an energy density of 65 Wh/Kg, nearly half of the primary model of LIBs commercialized by Exxon in 1978 (130 Wh/Kg) and one-third of global Sony LIBs (150–190 Wh/kg) [142,143]. After extensive research on increasing the energy density of LIBs in the early 2000s, this figure increased to around 250 Wh/kg, which was still significantly lower than the energy density of fossil fuels such as gasoline; this remained a key challenge in fully transitioning vehicles to EVs. Equation (3) is calculated based on an integrated function derived from the output voltage and input current, which have an inverse relationship with the mass of the cell:

$$E = \frac{1}{M} \int_0^{td} vi_{app} \quad (3)$$

where M = mass of a cell, v = output voltage, and i = input current [144].

Several factors impact the energy density of LIBs, such as primary materials, the type of electrolyte, material designs (thickness, porosity, and physical properties), and charge voltage [145]. Higher voltage can significantly improve the energy density of LIBs. However, this is not feasible, as the battery would face electrolyte decomposition or lattice instability, which occurs at 4.2 V vs. Li/Li⁺ [146,147]. Modifying anode materials is another sufficient way to significantly improve the energy density of LIBs, especially for carbon-based anodes. These methods mainly focus on optimizing anode electrodes' structural and electrochemical properties:

(a) Coating

Applying a thin layer of material to the surface of an anode can modify its electrochemical properties, enhancing performance and stability. Surface coating with an oxide, a conductive carbon, or a polymer stabilizes the SEI and improves cycle stability. This layer acts as protection to reduce electrode degradation during each charge cycle and eventually increases the overall energy density of batteries. For instance, applying a polydopamine (PDA) coating layer to graphite anodes has effectively increased the thermal stability of the SEI [148]. This method also showed promising results for silicon/carbon compositions. Even though this layer boosts SEI stability, it can also mitigate volume expansion, enhance capacity retention, and, ultimately, provide better cycle life and durability. Wang et al. prepared coated Si/C anodes, and they stated that the prepared electrode exhibited a capacity retention of 80.0% after 100 cycles, compared to only 4.3% for pristine silicon electrodes at 0.1 Ag⁻¹ [149].

There are other types of coating layers that could have the same effect on the performance of LIBs. Liu et al. focused on regenerating waste graphite from spent lithium-ion

batteries by coating them with an amorphous carbon layer. After purification and calcination at high temperatures, an amorphous-layer coating derived from asphalt was applied under high temperatures. The final graphite showed a specific capacity of 367.90 mAhg^{-1} at 0.1 C, retaining 271.85 mAhg^{-1} after 350 cycles, and 83.24% at 0.5 C [150]. The amorphous layer fills the holes and gaps in the graphite structure to regenerate its electrical conductivity, structural stability, and lithium-ion diffusion pathways to maintain standard retention capacity;

(b) Nanostructuring techniques

Creating nanostructure porous and hollow structures in carbonaceous materials is a promising method for enhancing the energy density and electrochemical performance of LIBs. These methods improve the surface area available for intercalation and decrease ion diffusion pathways, enhancing the structural stability of anode materials [151]. Recent developments have been widely studied by using the templating activation process and etching methods to produce specific pore sizes and functionalities. In a templating strategy, scientists employ solid molds, such as silica, where carbon precursors are impregnated and carbonized, the template is chemically removed, and the final product is a well-ordered porous carbon structure; this method is called a hard template [152,153]. On the other hand, soft-templating processes utilize self-assembled copolymers or surfactants, which enable better control over pore size and conductivity [154,155]. These strategies could increase the specific capacity of an anode to 600 mAhg^{-1} at 1 C.

(c) Hybrid composites and alloys

Combining carbonaceous materials with high-capacity materials such as silicon, metal oxide, and metal alloy has been considered a promising strategy. Extensive research has been conducted regarding Si/C composition, which shows that this material can significantly enhance the capacity of the anode electrode while utilizing carbon to mitigate volume expansion and improve conductivity [139,140,156–159]. The theoretical capacity of the composition can reach 4200 mAhg^{-1} , which is nearly 10 times more than that of graphite; this high capacity significantly increases the energy density of LIBs containing this electrode [159]. Tin is also another popular composition material for graphite, as it can boost the capacity and energy density of graphite notably while maintaining its structural stability and conductivity [160,161]. It may face exfoliation during intercalation, and this composition can be bound to an inactive material such as cobalt to avoid mechanical degradation. Figure 9 depicts the specific capacity (mAhg^{-1}) and specific energy density (Wh/kg) for eight different carbonaceous and composite anode materials, highlighting their performance potential in lithium-ion batteries [46,86,89,154,162–164].

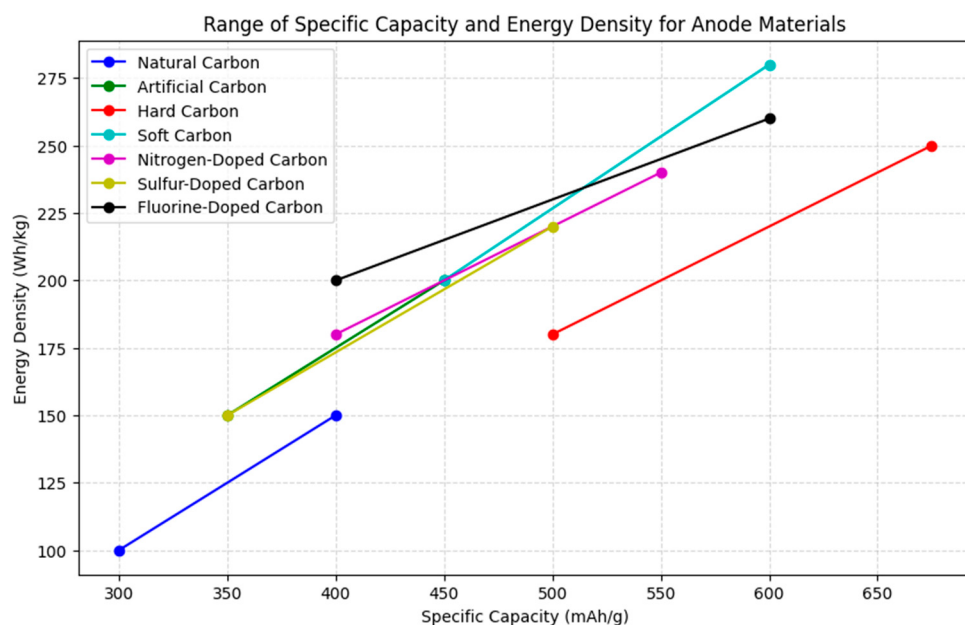
To summarize, Table 5 provides the experimental data for various types of anode modifications to increase energy density and capacity in LIBs.

Table 5. Experimental electrochemical properties of various anode materials for LIBs [65,78,156,165–177].

Anode Material	Initial Discharge Specific Capacity (mAhg^{-1})	C Rate	Voltage Range (V)	Retention Capacity	ICE (%)	Current Rate mAg^{-1}
Graphite	372	1	0.5–3	97% after 100 cycles	85.1	-
Bituminous coal artificial graphite	200–300	0.1	0–2	60–70% after 70 cycles	69.7–87.5	-
Modified artificial graphite	250	1	0.01–2	~90% after 40 cycles	~88.2	500
Pitch drive hard carbon	225.5	1	0–2	97% after 100 cycles	81.3	-
Soft carbon	278	1	0–3	74.3% after 300 cycles	70.2	600

Table 5. Cont.

Anode Material	Initial Discharge Specific Capacity (mAhg ⁻¹)	C Rate	Voltage Range (V)	Retention Capacity	ICE (%)	Current Rate mAg ⁻¹
Silicon/carbon composite	2900	-	-	37.9% after 600 cycles	-	400
Nitrogen-doped active carbon	397.78	0.1	0–2	~90% after 100 cycles	78.98	50
Nitrogen-doped graphene nanosheet	250	2.5	0.01–3	~100% after 10 cycles	~100	-
Sulfur-doped carbon	170	1	0–3	~96.8% after 100 cycles	60.6	-
Nitrogen and fluorine co-doped carbon	1075	-	0–3	~95% after 2000 cycles	56.7	100
PD-doped graphite	230	0.5	0.005–1.5	69% after 100 cycles	-	200
Graphene nanosheet	500	0.2	0–3	90% after 100 cycles	56	-
Boron-doped carbon	310	0.1	0–2	88% after 50 cycles	-	50

**Figure 9.** Comparison range of specific capacity and energy density for various anode materials in lithium-ion batteries [46,86,89,154,162,163].

3.4. Voltage (Cell Voltage) and SOC

Defining the voltage characteristics of carbonaceous anodes containing LIBs is essential for addressing key challenges and enhancing efficiency and battery performance. These anode materials operate at low voltage (~0.01–0.25 V vs. Li/Li⁺), resulting in maximizing energy density and reversibility. The anode materials can significantly impact the final voltage of LIBs by influencing the electrochemical potential difference between the anode and cathode, which directly determines the cell's operating voltage. Materials with low potential compared to lithium, such as graphite (~0.1 V vs. Li/Li⁺), provide a more significant voltage gap when paired with high-potential cathode materials, leading to higher energy density. On the other hand, anodes with higher potentials have lower overall cell voltages, and this high potential may lead to improving the safety and cycle life of LIBs. Therefore, choosing the anode material is critical and requires careful consideration, as it offers advantages and disadvantages.

The state of charge (SOC) is a crucial characterization in understanding the operational dynamics of LIBs, especially in the cell voltage profile domain. This value represents the ratio of charge or capacity stored to the battery's total capacity [178] and directly

impacts the voltage behavior of anode materials and, consequently, the battery's overall performance [179].

The voltage characteristics at varying SOC levels provide valuable insights regarding material reversibility, energy efficiency, and charge transfer kinetics; these parameters are expected to improve performance significantly. The voltage vs. SOC graph elaborates on how various anode materials impact the voltage profile of lithium-ion batteries, highlighting their operational characteristics [180]. By comparing the graph of different carbonaceous anode materials, it can be concluded that NG and AG comprise low and stable profiles; they would be ideal for maximizing energy density while also maintaining expectational long cycle life and enhanced safety. On the other hand, HCs and SCs exhibit broader working potential (~0.1–0.5 V vs. Li/Li⁺), resulting in better stability in specialized applications [166,181,182].

3.5. Internal Resistance and Impedance

Internal resistance is a critical factor that can significantly affect energy density, power delivery, heat generation, and, eventually, the overall performance of batteries. This resistance is made from various sources, such as electrochemical reaction kinetics, ionic transportation, and interfacial effects. The material properties, operating voltage, SOC, and battery cycle life influence it.

Internal resistance is composed of different types of resistance. **Ohmic resistance**, arising mainly from current collectors, electrolytes, and internal contacts, is minimized using highly conductive anodes [183]. **Charge transfer** resistance encompasses processes that depend on the surface area, the reaction kinetics at the anode–electrolyte interface, and the stability of the solid electrolyte interphase (SEI) [184]. It has been observed that charge transfer resistance increases significantly with aging cycles. Additionally, the charge transfer resistance and its growth rate are influenced by temperature and the state of charge (SOC) [185]. **The resistance of the SEI layer**, which is crucial for anode stabilization, is influenced by thickness, composition, and long-term stability. A well-formed SEI reduces resistance by preventing further electrolyte decomposition and maintaining efficient ion transport [186]. **Diffusion resistance** results from lithium-ion transport within the anode material and across the SEI layer; it becomes particularly significant at low temperatures or during high-rate cycling due to slower ion mobility. Diffusion resistance increases significantly as the SOC decreases; this finding signifies the avoidance of operating at low SOC levels (>20%) [187]. Finally, **polarization resistance**, caused by ion concentration gradients near the anode surface, increases under high-rate operations or when less-than-optimal electrolyte formulations are used, further impacting performance. This resistance increases significantly at high discharge rates and low ambient temperatures [187]. The distribution of types of resistance in anode electrode is depicted in Figure 10.

Based on Figure 10, it can be concluded that charge transfer resistance constitutes the largest portion of the overall internal resistance in the battery. This parameter is calculated using electrochemical impedance spectroscopy (EIS) and is derived from the Butler–Volmer (BV) equation (Equation (4)), written as

$$R_{ct} = \frac{RT}{2\alpha F I_0} \quad (4)$$

where R = the universal gas constant, T = absolute temperature (K), α = transfer coefficient, F = Faraday's constant, and I_0 = exchange density.

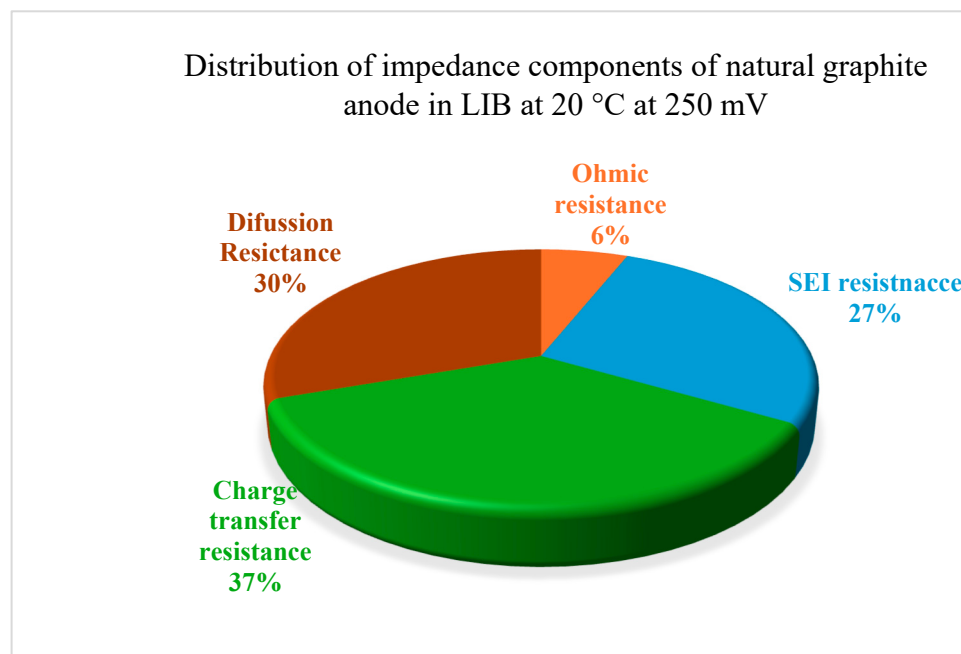


Figure 10. Distribution of impedance components of an NG anode in LIB at 20 °C and 250 mV [188].

To reduce this resistance, the charge transfer coefficient and exchange current density are key parameters to optimize, as they are directly related to this resistance and the battery's overall performance. The transfer coefficient can be increased by improving the kinetic reaction and reducing the activation energy for charge transfer. This parameter can be enhanced using modifications such as hetero-atom doping or electrode surface modifications.

Multiple strategies in LIBs can enhance exchange current density (I_0). Increasing the active surface area through nanostructure materials such as carbon nanotubes, graphene, and GO induces more reaction sites to the anode and leads to a higher I_0 . S-doping is also an efficient method that can increase the number of active sites and contribute greatly to decreasing overall internal resistance. Increasing electrode and ionic conductivity can also increase I_0 by accelerating the ion diffusion rates and reducing charge transfer resistance, facilitating faster lithium-ion transport and improving overall electrochemical reaction kinetics. Conductive additives are materials incorporated into LIB electrodes to enhance electrical conductivity and increase exchange current density. This material creates a continuous electron transport network, ensuring efficient flow across the electrode. Nam et al. prepared carbon black (CB)-containing anodes and studied their role in LIBs. Adding pre-lithiated CB to the graphite anode increased the initial ICE from 99% to 130% and directly impacted LIB internal resistance. A higher ICE indicates more cyclic reaction and lower irreversible capacity loss inside reactions. This results in a thinner and more stable SEI and can be a great sign of lower internal resistance, including charge transfer resistance [189].

3.6. Safety

LIBs are a millstone of energy storage systems, powering applications, EVs, and portable electronic devices. Since these high-energy-density devices are frequently used in daily life and come into direct contact with humans, ensuring the safety of these batteries remains an ongoing and critical challenge. Safety concerns may arise from different factors and operating conditions, such as thermal instability, electrochemical degradation, and mechanical malfunction. This failure may result in catastrophes such as thermal runaway, fires, or explosions [190]. Thermal runaway represents one of the most common and hazardous processes in LIBs. This phenomenon occurs when the heat generated in the

cell surpasses its ability to dissipate, resulting in a rapid temperature rise that deteriorates internal reactions. The thermal runaway process can be described in three stages. In stage 1, low-rate reactions begin at the anode ~ 90 °C, and at ~ 120 °C, significant degradation of the SEI layer occurs, exposing the lithiated graphite anode to electrolyte reduction, with the reaction rate steadily increasing. In stage 2, cathode degradation and side reactions start at around 150 °C (depending on the type of cathode material). Stage 3 involves high-rate runaway reactions, typically occurring at or above 180 °C. These reactions are mainly driven by oxygen generation from cathode decomposition and the subsequent oxidation of the electrolyte (Figure 11) [191].

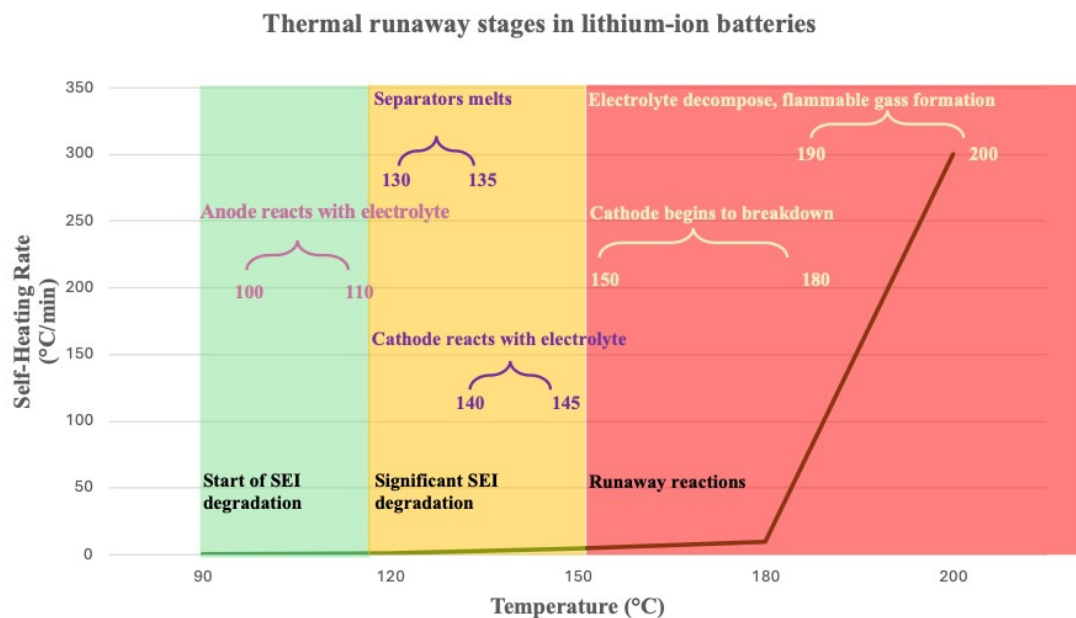


Figure 11. Thermal runaway stages in lithium-ion batteries.

To evaluate the progression of thermal runaway and quantify these stages, a study utilized an Accelerating Rate Calorimeter (ARC) in Heat-Wait-Seek (HWS) mode [192]. This method gradually heats the battery in an adiabatic environment and detects the onset of exothermic reactions when the self-heating rate exceeds a threshold, such as 0.02 °C/min [193].

In stage 1 (90–120 °C), the measured self-heating rate remains low, around 0.2 °C/min, indicating minor reactions such as SEI layer decomposition. In stage 2 (120–150 °C), the rate increases to 1–5 °C/min as significant electrolyte decomposition and gas venting occur. Stage 3 (150–200 °C and beyond) exhibits a dramatic surge in self-heating rates, exceeding 300 °C/min at 200 °C for half-charged cells (the SOC can impact this rate). This sudden intensification shows an uncontrollable thermal runaway that has already engaged with a strong oxygen-releasing and highly electrolyte-oxidative runaway reaction (Figure 11). The ARC data capture the intensity of thermal reactions and highlight the influence of the state of charge and temperature on the development of thermal runaway. These insights are critical in understanding LIB safety and designing mitigation strategies to prevent catastrophic failures.

A thermal runaway can significantly impact the capacity of LIBs by enhancing the growth of the SEI, which increases internal resistance and reduces active lithium ions. This capacity loss could deteriorate under high C rates and temperatures. Yang et al. stated that at 2 C, the relative capacity of a lithium iron phosphate (LiFePO₄) battery decreased by approximately 19.7% after 2000 cycles compared to at a 0.5 C rate. Similarly, higher ambient temperatures intensified capacity fade, with relative capacity dropping to 62.3% at

318.15 K, compared to 69.9% at 298.15 K [194]. On the other hand, at low temperatures, ion and charge transfer at the SEI would be disturbed and hindered. This phenomenon also led to capacity loss and primary material degradation, and, at around -20°C , the intercalation mechanism is almost entirely restricted [195].

There are miscellaneous causes of thermal runaway in lithium-ion batteries regarding cathode material decomposition [196,197], separator failure [198], overcharge, external mechanical abuse [199], manufacturing defects, and active material aging. Even though these also remain among the key factors contributing to most of the challenges experienced in efforts to ensure the safety of batteries, this paper focuses on safety issues related to carbonaceous anodes. Several factors related to the anode contribute to causing thermal runaway in LIBs.

Short-circuiting, caused by separator failure or the formation of dendrites, is one of the safety concerns regarding anodes. This happens when the cathode and anode make direct contact, triggering spontaneous chemical reactions, substantial heat generation, and the risk of fires or explosions. This phenomenon is a primary cause of thermal runaway and can result from physical collisions, the separator melting at high temperatures, or punctures by lithium dendrites. Mitigating internal short circuits can be carried out through improvements to the electrolyte, separator, and lithium anode, which are essential for avoiding thermal runaway [200]. Overcharging can also result in thermal runaway, as extensive charging can produce excessive heat, which eventually causes electrolyte and primary material decomposition. It is also worth noting that, compared to regular charging, overcharging causes more damage than over-discharging due to additional side effects and an increase in internal resistance, which leads to greater heating (nearly proportional to charging current); this induces more damage to the battery's efficiency [190,201].

Enhancing the thermal stability of carbon-based anode materials can significantly improve the safety profile of LIBs. The stability of the anode–electrolyte interface, particularly the SEI layer, plays a crucial role in preventing thermal runaway. Several modifications can increase this thermal stability by modifying anode–SEI interactions:

- (i) **Material design technique:** As discussed, the SEI layer plays an essential role in influencing the thermal runaway behavior of lithium-ion batteries. Therefore, one of the efficient strategies is to engineer a stable SEI layer with enhanced mechanical strength and chemical stability. Elemental doping and surface doping have been reported to be efficient in enhancing the thermal stability of these batteries [177,188,202–204]. These techniques can prevent side reactions by increasing temperature and maintaining structural integrity over extended cycles;
- (ii) **Using machine learning (ML):** Extensive datasets derived from electrolyte and anode properties can be effectively analyzed and comprehended by ML to maximize battery performance. Advanced models can simulate the dynamics of SEI formation under various conditions and provide insights into factors such as ion diffusion rates and reaction kinetics. Furthermore, ML anticipated the pattern of SEI decomposition as a function of time and facilitated the designing of materials that reduce heat generation and resist breakdown. This algorithm can be combined with battery management systems (BMSs) and provides insights that can effectively maximize the function of electrochemical parameters such as the SOC, C rates, ICE, and voltage limits to maintain SEI integrity [205–207].

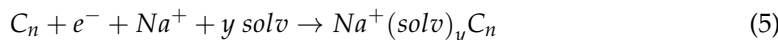
Wang et al. developed a machine learning (ML) model for a materials descriptor recommender to enhance predictions, such as, battery lifetime estimations and specific artificial graphite powder mechanisms. Such improvements can translate directly into LIB efficiency improvements by reducing the number of experimental trials, cutting material discovery time by nearly 40%, and increasing energy efficiency [205].

4. Sodium-Ion Batteries

4.1. Intercalation

The advent of sodium-ion batteries (SIBs) saw a potential alternative to LIBs in modern energy storage technology. These batteries gained more attention in the fields that required large-scale energy storage systems and renewable energy applications. These batteries are also known for being cost-effective and for their large raw material abundance (23,000 ppm Na vs. 17 ppm Li in the Earth's crust [208]), making them suitable for large-scale applications [209–211]. The larger ionic radius of sodium ions (compared to lithium ions) presents significant challenges in finding suitable anode materials, mainly graphite, which is widely used in LIBs. It is worth pointing out that, here, having a larger ionic radius is inaccurate, as potassium ions with a higher radius than sodium ions can be intercalated in graphite [212]. The most accurate scientific reason that graphite is not utilized in SIBs is the formation of thermodynamically unstable Na-GICs. The thermodynamic instability of Na-GICs is evident from their positive formation energy. The formation enthalpy of NaC_6 is +0.12 eV compared to –1.1 eV for LIBs, indicating that the formation of this compound is an endothermic and energetically unfavorable process, requiring energy input [213]. The weak cation interaction is also a solid reason for poor intercalation in Na-GIC. Chen et al. found that this weak intercalation arises from the competition between the ionization of the metal atom and ion–substrate coupling [214].

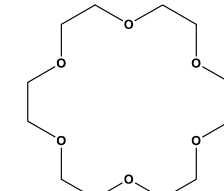
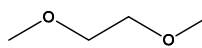
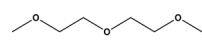
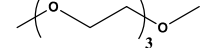
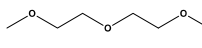
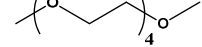
Recent studies, however, have proven that this intercalation can be made feasible by using solvated-Na-ion intercalation to form thermodynamically stable GICs, which is called the co-interaction mechanism. This mechanism can be written as Equation (5), in which C_n indicates the stage number and number of carbons in GIC, and solv represents the solvent molecule [215].



The co-intercalate solvent can enhance the reversibility and accelerate the kinetics of the graphite electrode, making it a promising advanced anode material for sodium-ion batteries. Moreover, co-intercalation can increase the space layer between graphite sheets. Kim et al. studied the expansion of graphite sheets, and, by analyzing XRD data, they reported that in SIBs containing diethylene glycol dimethyl ether, the interlayer spacing can increase to 11.62 Å compared to 3.35 Å for the pristine graphite spacing layer (Figure 12) [216].

Choosing a solvent could also be critical because it significantly affects intercalation behavior, ionic conductivity, and overall battery stability. Kim et al. investigated the solvated-ion intercalation of ternary Na–ether–graphite. They found that sodium intercalates through multiple staging reactions, forming first-stage graphite and stable GIC with a Na/C ratio of 1/28 to 1/21 and great reversibility. This sodium–ether complex ion can stack in parallel within the graphite sheets. They also discovered that the storage potential of sodium ions increased with the chain length of linear ether solvent molecules due to stronger screening effects, which reduce ion repulsion and enhance Na-ion solvation [217]. Herein, Table 6 provides the different solvents used in the recent study as a co-intercalate in SIBs [214,215,218–224].

Table 6. Study of sodium-ion co-intercalation in various solvents.

Solvent	Intercalation Compound	Capacity (mAhg ⁻¹)	C Rate	Reversibility	Observations	Solvent Molecule Structure	References
Crown ether	Na(crown) ₂ C _n	~75	0.2 C	Moderate	Limited by rigid ring structure, resulting in lower capacity and slower kinetics		[224]
Propylene carbonate + Monoglyme(PC+G1)	Na(mgly) ₂ C _n	~80–100	1 C	Moderate	Shows reversible sodium intercalation but limited stability compared to longer glymes		[222]
Diglyme	Na(digly) ₂ C _n	~100–110	1 C	High	Stable plateau with excellent co-intercalation of sodium ions, forming stable graphite layers		[223]
Triglyme	Na(trigly) ₂ C _n	~110–120	1 C	High	Reduced efficiency at room temperature; performs better at higher temperatures		[223]
Diethylene glycol dimethyl ether	Not applicable	~150	1 C	High	High reversibility and great mobility		[213]
Tetraglyme	Na(tetragly) ₂ C _n	~160–165	0.1 C	High	Stronger sodium-ion screening due to longer chains but at slightly higher intercalation voltages		[224]

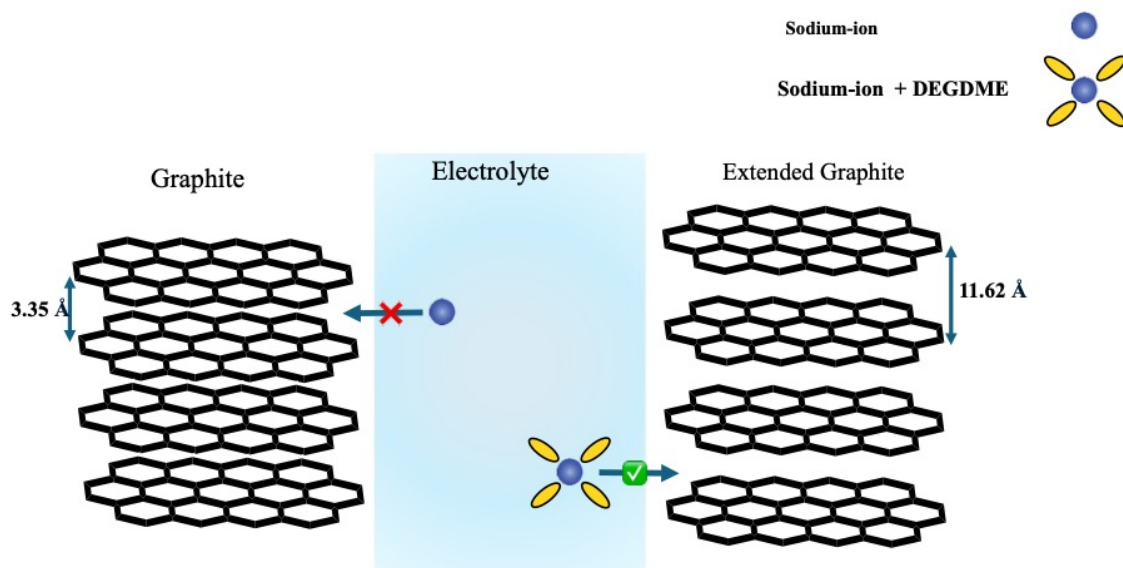


Figure 12. Intercalation and co-intercalation of sodium-ion in graphite.

Alternative intercalation methods have been investigated, such as using vapor phase reactions [225] and high-pressure reactions [224], to increase the capacity of graphite and form stable GICs; however, none of them have been efficient when compared to that of Li-GICs. Among all these methods, expanded graphite materials are considered one of the most effective approaches for enhancing sodium-ion storage. Wen et al. reported expanded graphite prepared through oxidation and the partial reduction of graphite. The final enlarged graphite had an interlayer lattice distance of 4.3 Å. The results show that this anode had excellent reversibility and a high reversible capacity of 284 mAhg^{-1} , with a retention of 73.92% after 2000 cycles [226]. Oxygen and oxygen-containing functional groups can boost the sodium-ion storage capacity of graphite by increasing the spacing layer and ion transport. On the other hand, graphite oxide (GO), with higher oxygen concentration (above 33%) and sizeable interlayer spacing ($\sim 0.61 \text{ nm}$), offers limited capacity ($\sim 156 \text{ mAhg}^{-1}$) owing to steric hindrance. Partially reduced expanded graphite (EG) achieves an optimal oxygen content (~10%) and interlayer spacing ($\sim 0.43 \text{ nm}$), which results in a higher reversible capacity ($\sim 300 \text{ mAhg}^{-1}$) and excellent cycling stability (73.92% retention over 2000 cycles) [185,226,227].

In this sense, Wen et al. studied the optimization of EG and its oxygen content. They have reported the exceptional performance of a graphite anode for SIBs, synthesized through oxidation followed by partial reduction. They prepared EG at 600°C over different periods (0 h, 1 h, and 5 h). The distance between the layers of each product was 0.61 nm, 0.43 nm, and 0.37 nm compared to pristine graphite with an interlayer spacing of 0.34 nm. As the oxidation period is extended, the oxygen concentration in EG initially decreases from 33% to 10% after 1 h and then to 8% after 5 h. The capacities obtained for each product were 13, 156, 300, and 100 mAhg^{-1} , corresponding to oxidation periods ranging from 0 to 5 h. It can be concluded that the concentration of oxygen and the interlayer spacing of EG should be optimized to obtain the maximum capacity [226,228].

Ma et al. used EG to prepare porous graphite nanostructures. In this method, EG first reacts with silicon vapor to form silicon carbide (SiC), followed by a selective chlorination process. This method yields products with exceptional stability, high conductivity, and a tangible porous structure. This structure also showed a long cycle life and a great capacity of 198 mAhg^{-1} at 0.1 Ag^{-1} while maintaining 67.2% capacity after 1000 cycles at 5 Ag^{-1} [49].

Doping graphite could also significantly increase its capacity and enhance sodium-ion storage capacity by improving electronic conductivity, preparing additional active sites,

and optimizing interlayer spacing, resulting in better sodium-ion intercalation. Nitrogen, as discussed, could result in a conductive network and more active site results that enhance the electrochemical performance of SIBs. Hu et al. increased the capacity and ICE of EG nitrogen doped in ether-based and ester-based electrolytes to around 125 mAhg^{-1} and 110 mAhg^{-1} , respectively, with a current density of 30 Ag^{-1} [229]. The types of modifications that can be performed on graphite to be able to intercalate with sodium are summarized in Figure 13.

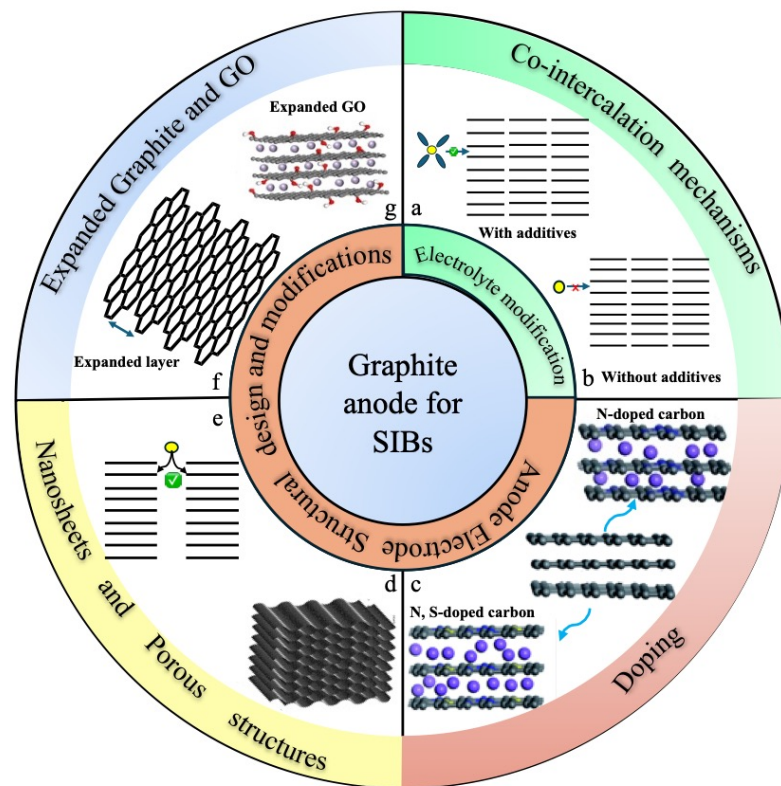


Figure 13. Schematic illustration of various design strategies and modifications for graphite anodes in SIBs: (a,b) co-intercalation mechanism of solvated sodium ions in graphite layers and the unsuccessful intercalation of sodium ions in graphite without a solvation shell; (c) hetero-atom doping to enhance sodium-ion storage capacity [230]; (d) nanostructured porous graphite sheets for enhanced ion diffusion and cycling stability [49]; (e) expanded graphite with porous structures; (f,g) graphene oxide (GO) structures as an anode material for SIBs [226].

While various intercalation mechanisms have been proposed for sodium-ion storage in graphite, the effectiveness of these methods varies significantly under different conditions. The co-intercalation method improves reversibility, but it is highly dependent on the type of solvent. While expanded graphite and graphite oxide balance capacity and stability, extensive oxidation can deteriorate the overall performance, and they also suffer from poor conductivity compared to pristine graphite. Nanosheets and nanoparticles have shown promising features, including enhancing conductivity and intercalation stabilization. However, challenges like volume expansion, nanoparticle dispersion, and scalability still exist. Considering all these concerns for each method, while nanoparticle and co-intercalant solvents showed promising results, expanded graphite stands out among others.

Apart from graphite, HC is another carbonaceous anode material widely utilized in SIBs. HCs are considered the most suitable anode material for SIBs because they have larger intralayer spacing than pristine graphite. The intercalation mechanism in HCs is quite different and still under debate. Bommier et al. studied this intercalation mechanism, and they have stated that the sodium-ion storage interaction mechanism comprises three

main stages: (1) the ions become stored at defect sites in sloping regions, (2) intercalation between graphene sheets in low-voltage plateau regions occurs, and, finally, (3) ions become adsorbed on pore surfaces [231]. HCs can be synthesized from different precursors through various procedures, such as pyrolysis. Zhong et al. prepared a biomass-derived HC anode for SIBs; they used multiple types of biomass precursors to synthesize HC over a temperature-controlled process. The capacity of the obtained hard carbon (HC) ranged from 210 to 430.5 mAhg^{-1} , with an initial Coulombic efficiency (ICE) varying between 21% and 89.1%, depending on the preparation methods and processing conditions [232].

HCs can be doped by various hetero-atoms to increase anode efficiency. Nitrogen doping is the most popular method of improving sodium ion absorption. Agrawal et al. prepared nitrogen-doped HC spheres through a hydrothermal process with ammonium as a nitrogen source. The final doped electrode has 286 mAhg^{-1} at 30 mAg^{-1} , almost 30% more than undoped spheres under the same condition [233]. It is worth pointing out that the cycle life and retention of hard carbon (HC) show only moderate improvement in this doping treatment. Another efficient method to increase durability while increasing capacity is the co-doped method of nitrogen and sulfur for HCs. Jin et al. prepared N and S co-doped carbon via the carbonization process of citrate sodium and thiourea. The optimized final product (NSC_2) exhibits a high reversible capacity of 280 mAhg^{-1} with a capacity retention of ~80% after 2000 cycles [234].

Compared to HCs, SCs offer lower capacity; however, they have better structural stability and conductivity. In the early stages of SIBs, Doeff et al. reported the ability of SC to accommodate sodium ions, form NaC_{24} GIC, and deliver 90 mAhg^{-1} capacity [235]. This material provides various capacities, primarily determined by the preparation method. The capacity typically ranges from 89 to 233 mAhg^{-1} , with an interlayer spacing between 3.46 \AA and 3.62 \AA , depending on the pyrolysis conditions used during synthesis [236].

4.2. Energy Density and Capacity

One of the main reasons that LIBs still dominate the rechargeable batteries market is the exertional energy density of these batteries compared to that of SIBs. This poor energy density arises from several inherent and electrode-related challenges. Larger ionic radii and a higher redox potential lead to lower cell voltage, side reactions, and unstable intercalation compounds, which are the leading causes of this matter. These factors are considered significant hurdles to achieving higher energy densities in SIBs [237]. Doping and selecting the appropriate precursor have been shown to significantly impact the energy density and capacity of HCs. To further address these challenges and maximize SIB efficiency, researchers have suggested several strategies, with surface control being one of the most effective approaches for optimizing battery performance.

Although the porous structure of HCs facilitates ion interaction, a higher number of active sites and an excessively porous structure lead to increased electrolyte decomposition and the formation of a thicker SEI, eventually leading to a dramatic decline in anode capacity [238]. It is also worth mentioning that sodium storage at lower plateau voltage is highly related to closed nanopores and other closed porous structures [239]. Therefore, increasing or decreasing the surface defects of HC is crucial, and they need to be controlled to achieve higher capacity and energy density while considering cycle life and safety issues.

Reducing surface defects in hard carbon (HC) is essential for boosting the performance of sodium-ion batteries, particularly by enhancing the ICE. Using coatings made from soft carbon(SC) precursors limits defect and oxygen-containing formation, achieving an ICE as high as 94.1% over 100 cycles with a capacity of $\sim 280 \text{ mAhg}^{-1}$ at 20 mAg^{-1} [240]. Reduction by hydrogen during hydrolysis is also another effective method to decrease the defects. Zhu et al. conducted an experiment and synthesized different types of HC reduced

by hydrogen. The final electrochemical result shows 286 to 400 mAhg^{-1} capacity with 65% to 80% retention (depending on the temperature HCs formed) in 300 cycles at 0.4 C [241].

On the other hand, hetero-atom doping is one of the most efficient ways to increase the capacity and energy density of HCs in SIBs by increasing surface defects. For instance, the presence of oxygen-containing atoms can improve sodium-ion intercalation, resulting in higher capacity. This method can make these batteries ideal for fast-charging applications, as the capacity remains high at a high current density [242].

Another surface-controlled method that could result in adjusting a closed porous structure is utilizing an auxiliary agent. Meng et al. researched a strategy to prepare a closed porous structure. They used phenol formaldehyde as the carbon source and ethanol as the pre-forming agent. Ethanol can produce steam to facilitate the development of cavities, which, later during the carbonization process, can be converted to closed pores in the final structure of HC. The final HC showed a specific capacity of 410 mAhg^{-1} with a Coulombic efficiency of 83% and an energy density of 300 Wh/kg at 0.1 C [243,244].

4.3. Safety

4.3.1. Thermal Runaway

As mentioned previously, SIBs are considered the most suitable alternative to LIBs. However, safety concerns, such as thermal runaway, remain the most prominent challenge for these batteries. Thermal runaway leads to the decomposition of the electrolyte, gas release, and even fires or explosions, especially when temperatures reach beyond 150 °C. Compared to LIBs, SIBs exhibit slower heat generation and lower exothermic intensity, enhancing their safety profile. Three primary sources for heat generation may result in a thermal runaway: (1) entropy changes in electrochemical reactions, (2) polarization heat, and (3) side reaction heat [245].

Robinson et al. suggested that the thermal runaway comprises four main stages. (1) Pre-stage: Intensive heat is generated from different sections, which depends on battery properties such as C rates, SOC energy density, etc. (2) Heat accumulation stage: This region can be regarded as the start of thermal runaway owing to an extensive side reaction. The SEI layer on the hard carbon anode at ~30 °C starts decomposing, which is initiated much sooner than in LIBs (around 90 °C). This step is followed by the reaction of electrolyte and anode materials at around ~120 °C, producing flammable gas. At ~130 °C, the separator starts melting down (this varies based on the material, up to 250 °C) [246]. At the end of this stage is the decomposition of cathode material, which is extremely exothermic and followed by oxygen production. (3) Thermal abuse: After cathode decomposition, heat generation becomes accelerated, and the self-heat rate reaches 10 °C/min. (4) Electrolyte combustion: This stage occurs at around 300 °C. The battery experiences complete structural and chemical breakdown at this point, leading to catastrophic failure [247].

4.3.2. Strategies to Enhance Safety Profile

The anode and electrolyte composition plays a crucial role in the thermal runaway of SIBs. The highly defective structure of HC, unstable sodium storage, and a reactive electrolyte at elevated temperatures can generate extensive heat and result in an explosion and thermal runaway. Several modifications focus on primary materials and anode–electrolyte interaction to minimize side effects and increase the safety profile of SIBs:

(i) Anode–electrolyte modification

Sodium clustering is one of the common side reactions on the anode surface, which refers to the formation of metallic-like sodium clusters in the nanopores and defect sites of HC during the intercalation process. This phenomenon results in thermal instability, performance degradation, dendrite formation, and high internal resistance due to the quasi-

metallic nature. Niu et al. investigated the safety features of SIBs by analyzing sodium clustering in the HC anode. They have found that SIBs have lower thermal stability than LIBs, with a self-heating onset and thermal runaway of 94 °C and 192 °C, respectively (compared to 102 °C and 233 °C for LIBs, respectively). Initially, they tried to solve the sodium clustering issue with electrolyte additives such as fluoroethylene carbonate (FEC). This additive-containing electrolyte helped to form a more stable SEI, but sodium clusters still triggered exothermic reactions. They have studied alternative types of materials, such as SC. The results showed a reduced effect and delayed thermal runaway but lower capacity than HC. The thermal runaway temperature of the final modified SC anode with additive-containing electrolyte increased from 192 °C to 233 °C, which greatly increases the safety profile of SIBs while maintaining high performance.

Using flame-retardant and non-flammable electrolytes can significantly reduce thermal runaway dangers. There have been considerable studies concerning changing electrolytes via additives to bypass thermal runaway. Zheng et al. prepared a non-flammable fluorinated carbonate electrolyte, demonstrating flame-reluctancy as fluorinated solvents have lower vapor pressure and would form a more stable SEI than common carbonate electrolytes. This also results in having a wider electrochemical window (~5.2 V compared to ~4.5 V in conventional carbonate electrolytes), reducing the risk of thermal runaway and explosion [248]. Vinylene carbonate is another common additive that positively impacts SIB safety by forming a durable, polymer-rich SEI, minimizing side reactions, and enhancing the stability of electrodes. Zhao et al. found that the internal resistance growth decreased by approximately 41.61% when adding 1 vol% vinylene carbonate (VC) [249];

(ii) Coating

Sodium-ion batteries (SIBs) rely on various coating techniques to improve their performance and safety by tackling issues such as structural stability. SCs can be coated on HC anodes, which significantly enhances these batteries' safety profile. This method solves safety challenges by addressing key risks such as thermal runaway, electrolyte decomposition, and mechanical instability. This layer eliminates defects and oxygen-containing functional groups, resulting in minimized side reactions that could trigger excessive heat generation and fire hazards. This method could also enhance the stability of the SEI layer and prevent uncontrolled sodium plating and clustering. Additionally, the SC coating layer improves conductivity, allowing for efficient heat dissipation, which significantly lowers the risk of overheating and thermal runaway [240,250].

The coating method is also applicable to cathode materials. Aluminum oxide and zinc oxide coating are the most popular cathode coating methods, which can help to avoid exfoliation and maintain consistent cycling performance [251,252]. Other types of coating layers have been suggested, such as NaPO₃, NaCaPO₄, Na₂Ti₃O₇, and conductive polymers [253–255];

(iii) Machine learning

Machine learning (ML) has significantly impacted the safety record of SIBs, specifically in optimizing anode material efficiency. ML algorithms can predict anode material behavior under various conditions and the most probable resolution determination by processing and collating much data regarding material behavior, electrochemical performance, and degradation trends. With such algorithms, one can opt for the most efficient surface treatments and doping methodologies for anode thermal steadiness and chemical durability improvement. Moreover, ML can simulate the development and steadiness of the solid electrolyte interphase (SEI), an essential feature in averting thermal runaway. Sekine et al. utilized ML to anticipate the ideal composition for SIBs, both for anodes and cathodes, based on the different databases derived from SIB performance. The result shows an increase

in thermal stability and reduced electrode degradation. This method could decrease the safety risk, particularly overheating and structural breakdown, by approximately 25–40%, which is much better than the traditional methods [256].

4.4. Comparison Between LIBs and SIBs

LIBs and SIBs are considered among the most efficient energy storage and utilization technologies. The early milestone of LIBs dates back to 1913, when Gilbert N. Lewis introduced the origins of lithium-ion batteries. However, he did not develop a practical LIB. These modern LIBs were officially developed later in the 1970s–1980s, with significant contributions from John B. Goodenough, Stanley Whittingham, and Akira Yoshino, resulting in Sony's commercialization of lithium-ion batteries in 1991. On the other hand, the early hypothesis of storing energy in SIBs originated in the late 1980s with G. Newman, which was followed by further development in the 2000s (Figure 14a). LIBs are experiencing market dominance and gaining more research attention due to their better performance and energy storage capacity (Figure 14b). However, these batteries are more expensive because lithium is less abundant than sodium, and its mining process requires more precision and sensitivity. Figure 14c compares the electrochemical performance and aging of the most ubiquitous anode materials for LIBs and SIBs. Considering the overall performance of each anode, it can be concluded that the most promising anode for LIBs is graphite, and, for SIBs, it is hard carbon (HC).

Lithium costs 5000 USD/ton compared to sodium, which costs 150 USD/ton [257]. LIBs achieve higher energy densities, ranging from 150 to 250 Wh/kg, which makes them suitable for applications requiring compact and lightweight energy storage. In contrast, SIBs have a lower energy density, typically between 100 and 150 Wh/kg, which allows them to be utilized in short-range EVs [179,258] (Table 7). It is still challenging to make SIBs as efficient as LIBs, and extensive research has been conducted revolving around this matter, such as modifying HCs or EG to fill this gap; however, it is insufficient to rely on SIBs entirely.

LIBs dominate the EV market, with popular EV cars such as the Tesla Model S, Nissan Leaf, and Chevrolet Bolt utilizing NMC or LFP with graphite anodes. SIBs are more favorable in budget-friendly EVs, such as the BYD Seagull and the JAC Sehol EX10, which contain sodium-ion cells with a lower range of 250–300 km compared to LIBs [257,259]. The environmental impact of LIBs is much more concerning and notable than SIBs. Lithium extraction is water-intensive and may result in soil degradation and natural and habitat destruction, eventually impacting our lives and health [260]. The reduced reliance on rare and expensive metals lowers the cost and minimizes the ecological impact of raw material extraction [261]. Additionally, the more straightforward chemistry of SIBs allows for potentially easier recycling processes, further enhancing their sustainability profile. Recycling LIBs is energy-intensive and expensive, costing 2 to 6 USD/kg [262]. LIBs are considered the leading choice for high-performance applications such as EVs. The manufacturing and recycling of these batteries are coupled with environmental concerns. This matter would intensify the essence of considering alternative methods for storing energy. SIBs offer sustainable, cost-effective solutions and can be a solution to this problem. More research and advancement would fill the gap between the efficiency of these types of batteries, resulting in the cheaper and safer use of stored energy.

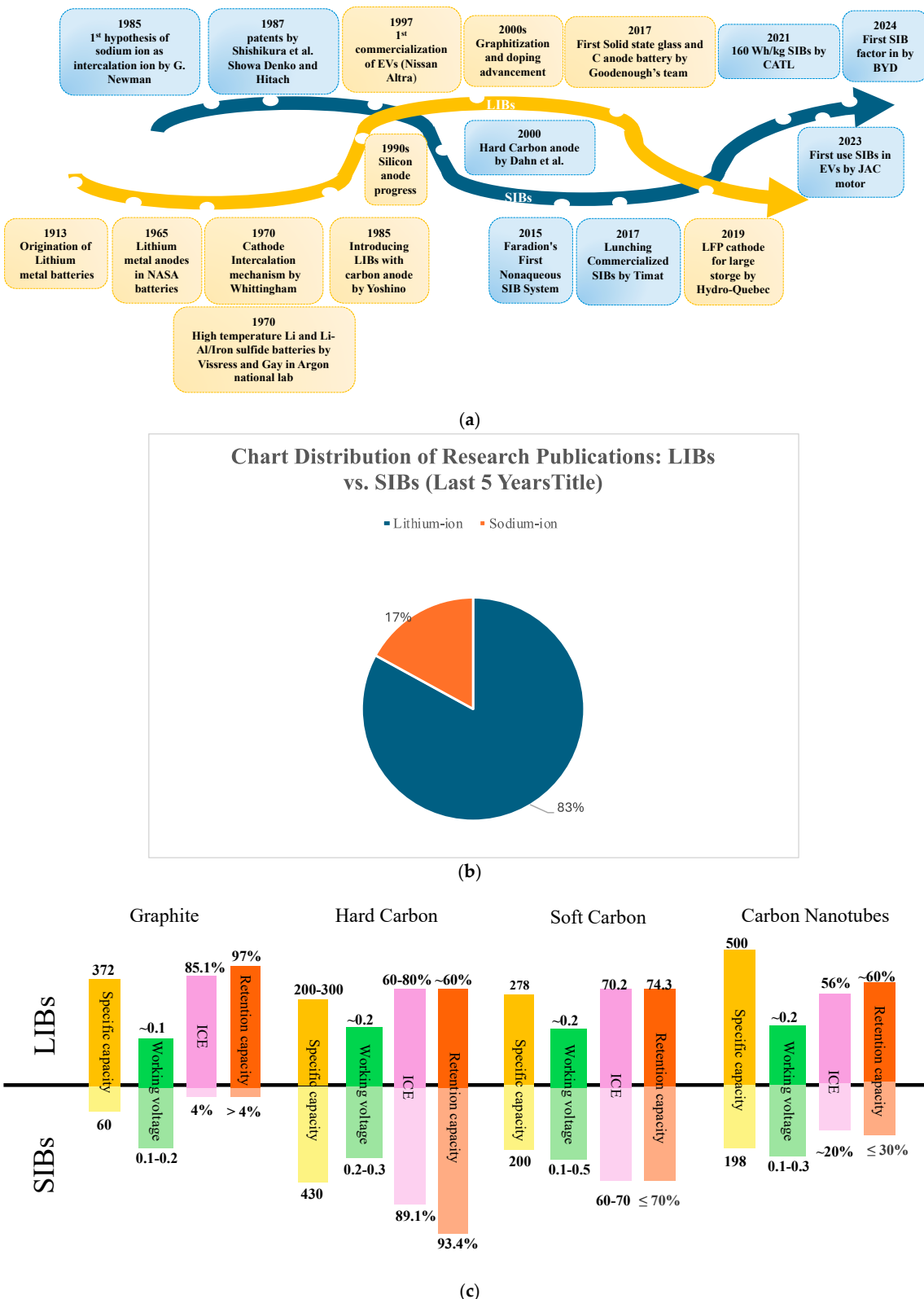


Figure 14. Comparison between LIBs and SIBs. (a) Milestones in the development of LIBs and SIBs. (b) Publication trends over the last five years: insights from Web of Science. (c) Electrochemical performance and capacity retention comparison of carbon-based anodes (retention capacity measured after 100 cycles) [132,263–268].

Table 7. Comparative analysis of various features in sodium- vs. lithium-ion batteries.

Features	LIBs	SIBs
Cation radius (\AA)	0.76	1.06
Abundance in Earth crust (ppm)	20	23,000
Density (g/cm^{-3})	0.534	0.97
Capacity (Wh/kg)	3829	1165
Electrode potential SHE (V)	-3.017	-2.71
Conductivity in EC/DEC (mS cm^{-1})	9.3	9.7
Cost (USD/ton)	5000	150
Maximum voltage (V)	4.2	3.6
Maximum energy density (V)	250	150
EV maximum distance (km)	600	300

References: [143,182,257,259,269–284].

5. Conclusions and Perspectives

Developing carbonaceous anode materials for LIBs and SIBs remains a critical area of research, driven by the demand for higher energy density, improved cycling stability, and cost-effectiveness. The dominant choice is still the rechargeable battery market, such as EVs and portable electronic devices, due to the high energy density, cycle life, and good overall performance of these batteries. However, there are some concerns regarding the limitation of lithium resources, which forces researchers to focus on alternative storage materials; among the alternative solutions, sodium-ion batteries can be a proper substitution because they are more abundant and have lower costs. These batteries also have promising electrochemical properties, such as high power density, specific capacity, and ICE, as well as a moderate cycle life. Despite these advantages, these batteries suffer from lower energy density and ion diffusion rates than LIBs. AG, NG, HC, and doped carbon materials have promising features in terms of conductivity, electrochemical properties, and cost-effectiveness and can contribute to the exceptional features of these batteries. AG exhibits high structural stability and a long cycle life, and HC provides better rate capability and enhanced sodium storage performance. Hetero-atom doping, such as nitrogen, sulfur, and fluorine doping, has further expanded the potential of carbonaceous materials by improving ion diffusion, electronic conductivity, reaction kinetics, and stability. Despite the extensive research and advancement, challenges remain, especially in optimizing the intercalation mechanism, increasing energy density and capacity, and producing cheaper anode materials.

Looking ahead, continued research and focus on the next-generation rechargeable batteries is crucial for overcoming the limitation of anode materials in LIBs and SIBs. The integration of machine learning and artificial intelligence can boost the pace of advancement in this field and revolutionize battery performance and safety. Future advancements should also focus on electrode–electrolyte interface engineering, with the development of stable SEI layers and electrolyte additives to minimize degradation and boost long-term cycling stability. Finding alternative doping methods for both LIBs and SIBs is crucial to enhancing electrode-specific capacity, optimizing intercalation kinetics, and improving structural stability. Furthermore, sustainable and scalable manufacturing methods will be crucial

for ensuring large-scale alternative materials and commercial viability. Various anode materials for both LIBs and SIBs can be optimized by integrating material design techniques, computational modeling, and various doping methods.

Additionally, recycling and increasing the sustainability of these batteries should increase, as these may have indispensable impacts on the environment and could ultimately influence our lives. While LIBs are the most prominent type of battery these days, it should not be forgotten that the primary source of this battery is running low, and a proper, reliable alternative needs to be substituted. SIBs hold strong potential for this; however, extensive research and focus must be applied to this battery to decrease the gap. Bridging this to achieve prominent SIB usage worldwide requires the further development of techniques and technologies, leveraging materials science, electrochemistry, and computational modeling to achieve higher performance, sustainability, and affordability while offering higher energy storage capacity.

Author Contributions: K.N. wrote the review manuscript and produced the graphics. A.K.M.R.R., M.V.R. and K.Z. designed the structure of the review, collected the papers related to the topic of the review, and completed the language corrections, with all authors contributing equally. All authors have read and agreed to the published version of the manuscript.

Funding: This research was funded by Nouveau Monde Graphite (NMG) in Quebec, Canada, Alliance-CNRC (Canadian government), and Prima (Quebec government).

Data Availability Statement: No new data were created or analyzed in this study. Data sharing is not applicable to this article.

Acknowledgments: The authors would like to thank Nouveau Monde Graphite (NMG) in Quebec, Canada, Alliance-CNRC (Canadian government), and Prima (Quebec government) for their financial support.

Conflicts of Interest: Author Mogalahalli Venkatasamy Reddy was employed by the company Nouveau Monde Graphite (NMG). The remaining authors declare that the research was conducted in the absence of any commercial or financial relationships that could be construed as a potential conflict of interest.

References

- Wang, J.; Azam, W. Natural Resource Scarcity, Fossil Fuel Energy Consumption, and Total Greenhouse Gas Emissions in Top Emitting Countries. *Geosci. Front.* **2024**, *15*, 101757. [[CrossRef](#)]
- Zhang, L.; Li, X.; Yang, M.; Chen, W. High-Safety Separators for Lithium-Ion Batteries and Sodium-Ion Batteries: Advances and Perspective. *Energy Storage Mater.* **2021**, *41*, 522–545. [[CrossRef](#)]
- Wang, M.; Wang, Q.; Ding, X.; Wang, Y.; Xin, Y.; Singh, P.; Wu, F.; Gao, H. The Prospect and Challenges of Sodium-Ion Batteries for Low-Temperature Conditions. *Interdiscip. Mater.* **2022**, *1*, 373–395. [[CrossRef](#)]
- Kumar Prajapati, A.; Bhatnagar, A. A Review on Anode Materials for Lithium/Sodium-Ion Batteries. *J. Energy Chem.* **2023**, *83*, 509–540. [[CrossRef](#)]
- Xiong, K.; Qi, T.; Zhang, X. Advancements in Graphite Anodes for Lithium-Ion and Sodium-Ion Batteries: A Review. *Electroanalysis* **2025**, *37*, e202400318. [[CrossRef](#)]
- Liu, C.; Sun, J.; Zheng, P.; Jiang, L.; Liu, H.; Chai, J.; Liu, Q.; Liu, Z.; Zheng, Y.; Rui, X. Recent Advances of Non-Lithium Metal Anode Materials for Solid-State Lithium-Ion Batteries. *J. Mater. Chem. A* **2022**, *10*, 16761–16778. [[CrossRef](#)]
- He, W.; Guo, W.; Wu, H.; Lin, L.; Liu, Q.; Han, X.; Xie, Q.; Liu, P.; Zheng, H.; Wang, L.; et al. Challenges and Recent Advances in High Capacity Li-Rich Cathode Materials for High Energy Density Lithium-Ion Batteries. *Adv. Mater.* **2021**, *33*, 2005937. [[CrossRef](#)]
- Olabi, A.G.; Abbas, Q.; Shinde, P.A.; Abdelkareem, M.A. Rechargeable Batteries: Technological Advancement, Challenges, Current and Emerging Applications. *Energy* **2023**, *266*, 126408. [[CrossRef](#)]
- Nzereogu, P.U.; Omah, A.D.; Ezema, F.I.; Iwuoha, E.I.; Nwanya, A.C. Anode Materials for Lithium-Ion Batteries: A Review. *Appl. Surf. Sci. Adv.* **2022**, *9*, 100233. [[CrossRef](#)]

10. Chen, Y.; Kang, Y.; Zhao, Y.; Wang, L.; Liu, J.; Li, Y.; Liang, Z.; He, X.; Li, X.; Tavajohi, N.; et al. A Review of Lithium-Ion Battery Safety Concerns: The Issues, Strategies, and Testing Standards. *J. Energy Chem.* **2021**, *59*, 83–99. [[CrossRef](#)]
11. Monteiro, I.F.; Silva, M.M.; Fidalgo-Marijuan, A.; Gonçalves, R.; Costa, C.M.; Lanceros-Mendez, S. Improving Lithium-Ion Battery Safety Through Separators with Thermal Shutdown Characteristics Induced by Thermal Expansion Microspheres. *J. Power Sources* **2025**, *631*, 236311. [[CrossRef](#)]
12. Wang, Z.; Wang, H.; Qi, S.; Wu, D.; Huang, J.; Li, X.; Wang, C.; Ma, J. Structural Regulation Chemistry of Lithium Ion Solvation for Lithium Batteries. *EcoMat* **2022**, *4*, e12200. [[CrossRef](#)]
13. Qiao, S.; Zhou, Q.; Ma, M.; Liu, H.K.; Dou, S.X.; Chong, S. Advanced Anode Materials for Rechargeable Sodium-Ion Batteries. *ACS Nano* **2023**, *17*, 11220–11252. [[CrossRef](#)] [[PubMed](#)]
14. Deng, L.; Wei, T.; Liu, J.; Zhan, L.; Chen, W.; Cao, J. Recent Developments of Carbon-Based Anode Materials for Flexible Lithium-Ion Batteries. *Crystals* **2022**, *12*, 1279. [[CrossRef](#)]
15. Sarfraz, N.; Kanwal, N.; Ali, M.; Ali, K.; Hasnain, A.; Ashraf, M.; Ayaz, M.; Ifthikar, J.; Ali, S.; Hendi, A.; et al. Materials Advancements in Solid-State Inorganic Electrolytes for Highly Anticipated All Solid Li-Ion Batteries. *Energy Storage Mater.* **2024**, *71*, 103619. [[CrossRef](#)]
16. Xu, G.; Jiang, M.; Li, J.; Xuan, X.; Li, J.; Lu, T.; Pan, L. Machine Learning-Accelerated Discovery and Design of Electrode Materials and Electrolytes for Lithium Ion Batteries. *Energy Storage Mater.* **2024**, *72*, 103710. [[CrossRef](#)]
17. Zhou, G.; Niu, C.; Kong, Y.; Wei, Z.; Wang, J.; Huang, Q.; Lu, H.; Zhang, Q. Research on Stimulation Responsive Electrolytes from the Perspective of Thermal Runaway in Lithium-Ion Batteries: A Review. *Fuel* **2024**, *368*, 131599. [[CrossRef](#)]
18. Ma, J.; Li, Z. Computational Design of Inorganic Solid-State Electrolyte Materials for Lithium-Ion Batteries. *Acc. Mater. Res.* **2024**, *5*, 523–532. [[CrossRef](#)]
19. Majid, A.; Najam, U.; Ahmad, S.; Alkhedher, M. On the Prospects of Using B_4C_3 as a Potential Electrode Material for Lithium-Ion Batteries. *Mater. Sci. Semicond. Process.* **2024**, *176*, 108320. [[CrossRef](#)]
20. Zhao, L.; Hu, Z.; Lai, W.; Tao, Y.; Peng, J.; Miao, Z.; Wang, Y.; Chou, S.; Liu, H.; Dou, S. Hard Carbon Anodes: Fundamental Understanding and Commercial Perspectives for Na-Ion Batteries beyond Li-Ion and K-Ion Counterparts. *Adv. Energy Mater.* **2021**, *11*, 2002704. [[CrossRef](#)]
21. Reddy, M.V.; Mauger, A.; Julien, C.M.; Paoletta, A.; Zaghib, K. Brief History of Early Lithium-Battery Development. *Materials* **2020**, *13*, 1884. [[CrossRef](#)] [[PubMed](#)]
22. Chen, C.; Wu, M.; Wang, Y.; Zaghib, K. Insights into Pseudographite-Structured Hard Carbon with Stabilized Performance for High Energy K-Ion Storage. *J. Power Sources* **2019**, *444*, 227310. [[CrossRef](#)]
23. Yu, P.; Tang, W.; Wu, F.-F.; Zhang, C.; Luo, H.-Y.; Liu, H.; Wang, Z.-G. Recent Progress in Plant-Derived Hard Carbon Anode Materials for Sodium-Ion Batteries: A Review. *Rare Met.* **2020**, *39*, 1019–1033. [[CrossRef](#)]
24. Jara, A.D.; Betemariam, A.; Woldetinsae, G.; Kim, J.Y. Purification, Application and Current Market Trend of Natural Graphite: A Review. *Int. J. Min. Sci. Technol.* **2019**, *29*, 671–689. [[CrossRef](#)]
25. Dresselhaus, M.S.; Dresselhaus, G. Intercalation Compounds of Graphite. *Adv. Phys.* **2002**, *51*, 1–186. [[CrossRef](#)]
26. Chang, H.; Wu, Y.-R.; Han, X.; Yi, T.-F. Recent Developments in Advanced Anode Materials for Lithium-Ion Batteries. *Energy Mater.* **2022**, *1*, 100003. [[CrossRef](#)]
27. Thauer, E.; Ottmann, A.; Schneider, P.; Möller, L.; Deeg, L.; Zeus, R.; Wilhelmi, F.; Schlestein, L.; Neef, C.; Ghunaim, R.; et al. Filled Carbon Nanotubes as Anode Materials for Lithium-Ion Batteries. *Molecules* **2020**, *25*, 1064. [[CrossRef](#)] [[PubMed](#)]
28. Li, Y.; Vasileiadis, A.; Zhou, Q.; Lu, Y.; Meng, Q.; Li, Y.; Ombrini, P.; Zhao, J.; Chen, Z.; Niu, Y.; et al. Author Correction: Origin of Fast Charging in Hard Carbon Anodes. *Nat. Energy* **2024**, *9*, 357. [[CrossRef](#)]
29. Yu, P.; Li, Z.; Zhang, D.; Xiong, Q.; Yu, J.; Zhi, C. Hierarchical Yolk-Shell Silicon/Carbon Anode Materials Enhanced by Vertical Graphene Sheets for Commercial Lithium-Ion Battery Applications. *Adv. Funct. Mater.* **2025**, *35*, 2413081. [[CrossRef](#)]
30. Peters, J.F.; Peña Cruz, A.; Weil, M. Exploring the Economic Potential of Sodium-Ion Batteries. *Batteries* **2019**, *5*, 10. [[CrossRef](#)]
31. Vaalma, C.; Buchholz, D.; Weil, M.; Passerini, S. A Cost and Resource Analysis of Sodium-Ion Batteries. *Nat. Rev. Mater.* **2018**, *3*, 18013. [[CrossRef](#)]
32. Ding, J.; Ji, D.; Yue, Y.; Smedskjaer, M.M. Amorphous Materials for Lithium-Ion and Post-Lithium-Ion Batteries. *Small* **2024**, *20*, 2304270. [[CrossRef](#)]
33. Liu, C.-F.; Liu, Y.-C.; Yi, T.-Y.; Hu, C.-C. Carbon Materials for High-Voltage Supercapacitors. *Carbon* **2019**, *145*, 529–548. [[CrossRef](#)]
34. Kim, M.I.; Cho, J.H.; Hwang, J.U.; Bai, B.C.; Im, J.S. Preparation of High-Crystallinity Synthetic Graphite from Hard Carbon-Based Carbon Black. *Appl. Phys. A* **2021**, *127*, 156. [[CrossRef](#)]
35. Xia, P.; Qin, Z.; Jing, S.; Li, S.; Peng, X.; Yuan, L.; Lu, S.; Zhang, Y.; Fan, H. Polymer Derived Mesoporous Hard Carbon Nanospheres as High-Performance Anode Materials for Potassium-Ion Batteries. *Colloids Surf. Physicochem. Eng. Asp.* **2024**, *701*, 134807. [[CrossRef](#)]
36. Alvira, D.; Antorán, D.; Manyà, J.J. Plant-Derived Hard Carbon as Anode for Sodium-Ion Batteries: A Comprehensive Review to Guide Interdisciplinary Research. *Chem. Eng. J.* **2022**, *447*, 137468. [[CrossRef](#)]

37. Li, X.; Ding, C.; Liang, Q.; Hu, J.; Xu, L.; Li, Y.; Liu, Y.; Gao, Y. Progress in Hard Carbons for Sodium-Ion Batteries: Microstructure, Sodium Storage Mechanism and Initial Coulombic Efficiency. *J. Energy Storage* **2024**, *98*, 112986. [CrossRef]
38. Wang, K.; Xu, Y.; Li, Y.; David, V.; Wu, J.; Huang, Y. Sodium Storage in Hard Carbon with Curved Graphene Platelets as the Basic Structural Units. *J. Mater. Chem. A* **2019**, *7*, 3327–3335. [CrossRef]
39. Ren, N.; Wang, L.; He, X.; Zhang, L.; Dong, J.; Chen, F.; Xiao, J.; Pan, B.; Chen, C. High ICE Hard Carbon Anodes for Lithium-Ion Batteries Enabled by a High Work Function. *ACS Appl. Mater. Interfaces* **2021**, *13*, 46813–46820. [CrossRef]
40. Zheng, H.; Zeng, J.; Wan, X.; Song, X.; Peng, C.; Wang, J.; Sun, L.; Wang, H.; Zhu, M.; Liu, J. ICE Optimization Strategies of Hard Carbon Anode for Sodium-Ion Batteries: From the Perspective of Material Synthesis. *Mater. Futur.* **2024**, *3*, 032102. [CrossRef]
41. Chu, Y.; Zhang, J.; Zhang, Y.; Li, Q.; Jia, Y.; Dong, X.; Xiao, J.; Tao, Y.; Yang, Q. Reconfiguring Hard Carbons with Emerging Sodium-Ion Batteries: A Perspective. *Adv. Mater.* **2023**, *35*, 2212186. [CrossRef]
42. Guo, X.; Xue, Y.; Zhou, H.; Weng, Y.; Zhou, J. Achieving Slope-Reigned Na-Ion Storage in Carbon Nanofibers by Constructing Defect-Rich Texture by a Cu-Activation Strategy. *ACS Appl. Mater. Interfaces* **2020**, *12*, 2407–2416. [CrossRef]
43. Chen, D.; Zhang, W.; Luo, K.; Song, Y.; Zhong, Y.; Liu, Y.; Wang, G.; Zhong, B.; Wu, Z.; Guo, X. Hard Carbon for Sodium Storage: Mechanism and Optimization Strategies Toward Commercialization. *Energy Environ. Sci.* **2021**, *14*, 2244–2262. [CrossRef]
44. Zhang, L.; Wang, W.; Lu, S.; Xiang, Y. Carbon anode materials: A detailed comparison between Na-ion and K-ion batteries. *Adv. Energy Mater.* **2021**, *11*, 2003640. [CrossRef]
45. Li, X.; Zhao, H.; Zhang, C.; Xing, B.; Zhang, C.; Zhou, C. One-Pot Fabrication of Pitch-Derived Soft Carbon with Hierarchical Porous Structure and Rich Sp₂ Carbon for Sodium-Ion Battery. *J. Mater. Sci. Mater. Electron.* **2021**, *32*, 21944–21956. [CrossRef]
46. Ghosh, S.; Zaid, M.; Dutta, J.; Parvin, M.; Martha, S.K. Soft Carbon in Non-Aqueous Rechargeable Batteries: A Review of Its Synthesis, Carbonization Mechanism, Characterization, and Multifarious Applications. *Energy Adv.* **2024**, *3*, 1167–1195. [CrossRef]
47. Tang, Z.; Zhou, S.; Huang, Y.; Wang, H.; Zhang, R.; Wang, Q.; Sun, D.; Tang, Y.; Wang, H. Improving the Initial Coulombic Efficiency of Carbonaceous Materials for Li/Na-Ion Batteries: Origins, Solutions, and Perspectives. *Electrochem. Energy Rev.* **2023**, *6*, 8. [CrossRef]
48. Onnerud, P.; Shi, J.; Chamberlain, R.; Singh, S.K.; Barnett, B.; Lampe-Onnerud, C. Benchmarking Graphite Materials Used as Anodes in Lithium-Ion Batteries. Available online: <https://www.google.com.hk/url?sa=t&source=web&rct=j&opi=89978449&url=https://www.electrochem.org/dl/ma/201/pdfs/0122.pdf&ved=2ahUKEwjR9J3msJuMAxXCsVYBHXOhM4UQFnoECBYQAQ&usg=AOvVaw3Ilqnglzs8KQhQvMsmzNRf> (accessed on 20 February 2025).
49. Ma, C.; Fan, Q.; Dirican, M.; Song, Y.; Zhang, X.; Shi, J. Porous Carbon Nanosheets Derived from Expanded Graphite for Supercapacitors and Sodium-Ion Batteries. *J. Mater. Sci.* **2020**, *55*, 16323–16333. [CrossRef]
50. GRAPHITE MARKET. Available online: <https://westwaterresources.net/minerals-portfolio/graphite-market/> (accessed on 20 February 2025).
51. Mine Production of Graphite Worldwide from 2010 to 2024 (in 1000 Metric Tons). Available online: <https://www.statista.com/statistics/1005851/global-graphite-production/> (accessed on 20 February 2025).
52. U.S. Geological Survey. Mineral Commodity Summaries 2024. Available online: <https://pubs.usgs.gov/publication/mcs2024> (accessed on 20 February 2025).
53. Qiao, Y.; Zhao, H.; Shen, Y.; Li, L.; Rao, Z.; Shao, G.; Lei, Y. Recycling of Graphite Anode from Spent Lithium-Ion Batteries: Advances and Perspectives. *EcoMat* **2023**, *5*, e12321. [CrossRef]
54. Meng, Y.; Li, J.; Gu, S.; Fu, Y.; Wang, Z.; Liu, J.; Gong, X. Li-Ion Complex Enhances Interfacial Lowest Unoccupied Molecular Orbital for Stable Solid Electrolyte Interface of Natural Graphite Anode. *Electrochim. Acta* **2023**, *449*, 142262. [CrossRef]
55. Shen, Y.; Shen, X.; Yang, M.; Qian, J.; Cao, Y.; Yang, H.; Luo, Y.; Ai, X. Achieving Desirable Initial Coulombic Efficiencies and Full Capacity Utilization of Li-Ion Batteries by Chemical Prelithiation of Graphite Anode. *Adv. Funct. Mater.* **2021**, *31*, 2101181. [CrossRef]
56. Asenbauer, J.; Eisenmann, T.; Kuenzel, M.; Kazzazi, A.; Chen, Z.; Bresser, D. The Success Story of Graphite as a Lithium-Ion Anode Material—Fundamentals, Remaining Challenges, and Recent Developments Including Silicon (Oxide) Composites. *Sustain. Energy Fuels* **2020**, *4*, 5387–5416. [CrossRef]
57. Gallego, N.C.; Contescu, C.I.; Meyer, H.M.; Howe, J.Y.; Meisner, R.A.; Payzant, E.A.; Lance, M.J.; Yoon, S.Y.; Denlinger, M.; Wood, D.L. Advanced Surface and Microstructural Characterization of Natural Graphite Anodes for Lithium Ion Batteries. *Carbon* **2014**, *72*, 393–401. [CrossRef]
58. Yang, Y.; Zou, Y.-C.; Woods, C.R.; Shi, Y.; Yin, J.; Xu, S.; Ozdemir, S.; Taniguchi, T.; Watanabe, K.; Geim, A.K.; et al. Stacking Order in Graphite Films Controlled by van Der Waals Technology. *Nano Lett.* **2019**, *19*, 8526–8532. [CrossRef] [PubMed]
59. Zhao, W.; Zhao, C.; Wu, H.; Li, L.; Zhang, C. Progress, Challenge and Perspective of Graphite-Based Anode Materials for Lithium Batteries: A Review. *J. Energy Storage* **2024**, *81*, 110409. [CrossRef]
60. Li, Y.; Lu, Y.; Adelhelm, P.; Titirici, M.-M.; Hu, Y.-S. Intercalation Chemistry of Graphite: Alkali Metal Ions and Beyond. *Chem. Soc. Rev.* **2019**, *48*, 4655–4687. [CrossRef]

61. Kim, Y.; Jeong, E.H.; Kim, B.S.; Park, J.D. Comparative Study on the Rheological Properties of Natural and Synthetic Graphite-Based Anode Slurries for Lithium-Ion Batteries. *Korea-Aust. Rheol. J.* **2024**, *36*, 25–32. [CrossRef]
62. Zhao, Y.; Fu, Y.; Meng, Y.; Wang, Z.; Liu, J.; Gong, X. Challenges and Strategies of Lithium-Ion Mass Transfer in Natural Graphite Anode. *Chem. Eng. J.* **2024**, *480*, 148047. [CrossRef]
63. Hupp, T.R.; Lewis, I.C.; Criscione, J.M.; Reddy, R.L.; Fulgenzi, C.F.; Page, D.J.; Fisher, F.F.; Dzermejko, A.J.; Hedge, J.B. Graphite, Artificial. In *Kirk-Othmer Encyclopedia of Chemical Technology*; Kirk-Othmer, Ed.; Wiley: Hoboken, NJ, USA, 2003; ISBN 978-0-471-48494-3.
64. Chen, Z.; Li, Y.; Wang, L.; Wang, Y.; Chai, J.; Du, J.; Li, Q.; Rui, Y.; Jiang, L.; Tang, B. A Comprehensive Review of Various Carbonaceous Materials for Anodes in Lithium-Ion Batteries. *Dalton Trans.* **2024**, *53*, 4900–4921. [CrossRef]
65. Wang, S.; Li, Y.; Wang, L.; Qiao, Y.; Xu, J.; Li, J.; Zhang, S. PVA Generated Carbon-Coated Natural Graphite Anode Material for Enhanced Performances of Lithium-Ion Batteries. *Ionics* **2024**, *30*, 6845–6853. [CrossRef]
66. Yoshio, M.; Wang, H.; Fukuda, K. Spherical Carbon-Coated Natural Graphite as a Lithium-Ion Battery-Anode Material. *Angew. Chem. Int. Ed.* **2003**, *42*, 4203–4206. [CrossRef]
67. Fischer, S.; Doose, S.; Müller, J.; Höfels, C.; Kwade, A. Impact of Spheroidization of Natural Graphite on Fast-Charging Capability of Anodes for LIB. *Batteries* **2023**, *9*, 305. [CrossRef]
68. Qi, H.; Shi, X.; Liu, Z.; Yan, Z.; Sun, Z. In Situ Etched Graphite Felt Modified with CuFe₂O₄/Cu₂O/Cu Catalyst Derived from CuFe PBA for the Efficient Removal of Sulfamethoxazole Through a Heterogeneous Electro-Fenton Process. *Appl. Catal. B Environ.* **2023**, *331*, 122722. [CrossRef]
69. Lund, S.; Kauppila, J.; Sirkä, S.; Palosaari, J.; Eklund, O.; Latonen, R.-M.; Smått, J.-H.; Peltonen, J.; Lindfors, T. Fast High-Shear Exfoliation of Natural Flake Graphite with Temperature Control and High Yield. *Carbon* **2021**, *174*, 123–131. [CrossRef]
70. Soldatos, J. (Ed.) *Artificial Intelligence In Manufacturing: Enabling Intelligent, Flexible and Cost-Effective Production Through AI*; Springer: Cham, Switzerland, 2024; Available online: <https://library.oapen.org/handle/20.500.12657/87623> (accessed on 20 February 2025).
71. Weimer, A.W. (Ed.) *Carbide, Nitride and Boride Materials Synthesis and Processing*, 1st ed.; Chapman & Hall: London, UK; Weinheim, Germany, 1997; ISBN 978-0-412-54060-8.
72. Lee, S.-M.; Kang, D.-S.; Roh, J.-S. Bulk Graphite: Materials and Manufacturing Process. *Carbon Lett.* **2015**, *16*, 135–146. [CrossRef]
73. Hwang, J.U.; Cho, J.H.; Lee, J.D.; Im, J.S. Characteristics of an Artificial Graphite Anode Material for Rapid Charging: Manufactured with Different Coke Particle Sizes. *J. Mater. Sci. Mater. Electron.* **2022**, *33*, 20095–20105. [CrossRef]
74. Ōya, A.; Marsh, H. Phenomena of Catalytic Graphitization. *J. Mater. Sci.* **1982**, *17*, 309–322. [CrossRef]
75. Kulkarni, S.; Huang, T.-Y.; Thapaliya, B.P.; Luo, H.; Dai, S.; Zhao, F. Prospective Life Cycle Assessment of Synthetic Graphite Manufactured via Electrochemical Graphitization. *ACS Sustain. Chem. Eng.* **2022**, *10*, 13607–13618. [CrossRef]
76. Jin, X.; He, R.; Dai, S. Electrochemical Graphitization: An Efficient Conversion of Amorphous Carbons to Nanostructured Graphites. *Chem.-Eur. J.* **2017**, *23*, 11455–11459. [CrossRef]
77. Mohamed, A.M.A.; Dong, S.; Elhefnawey, M.; Dong, G.; Gao, Y.; Zhu, K.; Cao, D. A Comparison of the Electrochemical Performance of Graphitized Coal Prepared by High-Temperature Heating and Flash Joule Heating as an Anode Material for Lithium and Potassium Ion Batteries. *Chem. Phys. Lett.* **2023**, *815*, 140362. [CrossRef]
78. Xing, B.; Zhang, C.; Cao, Y.; Huang, G.; Liu, Q.; Zhang, C.; Chen, Z.; Yi, G.; Chen, L.; Yu, J. Preparation of Synthetic Graphite from Bituminous Coal as Anode Materials for High Performance Lithium-Ion Batteries. *Fuel Process. Technol.* **2018**, *172*, 162–171. [CrossRef]
79. Shi, M.; Song, C.; Tai, Z.; Zou, K.; Duan, Y.; Dai, X.; Sun, J.; Chen, Y.; Liu, Y. Coal-Derived Synthetic Graphite with High Specific Capacity and Excellent Cyclic Stability as Anode Material for Lithium-Ion Batteries. *Fuel* **2021**, *292*, 120250. [CrossRef]
80. Wang, T.; Wang, Y.; Cheng, G.; Ma, C.; Liu, X.; Wang, J.; Qiao, W.; Ling, L. Catalytic Graphitization of Anthracite as an Anode for Lithium-Ion Batteries. *Energy Fuels* **2020**, *34*, 8911–8918. [CrossRef]
81. Thapaliya, B.P.; Luo, H.; Halstenberg, P.; Meyer, H.M.; Dunlap, J.R.; Dai, S. Low-Cost Transformation of Biomass-Derived Carbon to High-Performing Nano-Graphite via Low-Temperature Electrochemical Graphitization. *ACS Appl. Mater. Interfaces* **2021**, *13*, 4393–4401. [CrossRef]
82. Liu, M.; Shi, H.; Guo, L.; Fang, Z.; Chen, D.; Li, W.; Deng, B.; Li, W.; Du, K.; Yin, H.; et al. Enhanced Graphitization of CO₂-Derived Carbon Anodes via Joule Heating Reformation for High-Performance Lithium-Ion Batteries. *Carbon* **2025**, *232*, 119781. [CrossRef]
83. AbdelHamid, A.A.; Mendoza-Garcia, A.; Ying, J.Y. Advances in and Prospects of Nanomaterials' Morphological Control for Lithium Rechargeable Batteries. *Nano Energy* **2022**, *93*, 106860. [CrossRef]
84. Xia, Q.; Liu, H.; Zhao, X.S. Surface Engineering of Anode Materials for Improving Sodium-Ion Storage Performance. *J. Mater. Chem. A* **2022**, *10*, 3889–3904. [CrossRef]
85. Cheng, Q.; Yuge, R.; Nakahara, K.; Tamura, N.; Miyamoto, S. KOH Etched Graphite for Fast Chargeable Lithium-Ion Batteries. *J. Power Sources* **2015**, *284*, 258–263. [CrossRef]
86. Yuan, Y.; Chen, Z.; Yu, H.; Zhang, X.; Liu, T.; Xia, M.; Zheng, R.; Shui, M.; Shu, J. Heteroatom-Doped Carbon-Based Materials for Lithium and Sodium Ion Batteries. *Energy Storage Mater.* **2020**, *32*, 65–90. [CrossRef]

87. Yang, M.; Zhou, Z. Recent Breakthroughs in Supercapacitors Boosted by Nitrogen-Rich Porous Carbon Materials. *Adv. Sci.* **2017**, *4*, 1600408. [CrossRef] [PubMed]
88. Lee, W.J.; Lim, J.; Kim, S.O. Nitrogen Dopants in Carbon Nanomaterials: Defects or a New Opportunity? *Small Methods* **2017**, *1*, 1600014. [CrossRef]
89. Li, Y.; Chen, M.; Liu, B.; Zhang, Y.; Liang, X.; Xia, X. Heteroatom Doping: An Effective Way to Boost Sodium Ion Storage. *Adv. Energy Mater.* **2020**, *10*, 2000927. [CrossRef]
90. Wang, L.; Yang, Z.; Nie, H.; Gu, C.; Hua, W.; Xu, X.; Chen, X.; Chen, Y.; Huang, S. A Lightweight Multifunctional Interlayer of Sulfur–Nitrogen Dual-Doped Graphene for Ultrafast, Long-Life Lithium–Sulfur Batteries. *J. Mater. Chem. A* **2016**, *4*, 15343–15352. [CrossRef]
91. Zhang, T.; Li, C.; Wang, F.; Noori, A.; Mousavi, M.F.; Xia, X.; Zhang, Y. Recent Advances in Carbon Anodes for Sodium-Ion Batteries. *Chem. Rec.* **2022**, *22*, e202200083. [CrossRef] [PubMed]
92. Inagaki, M.; Toyoda, M.; Soneda, Y.; Morishita, T. Nitrogen-Doped Carbon Materials. *Carbon* **2018**, *132*, 104–140. [CrossRef]
93. Kim, D.-Y.; Li, O.L.; Kang, J. Novel Synthesis of Highly Phosphorus-Doped Carbon as an Ultrahigh-Rate Anode for Sodium Ion Batteries. *Carbon* **2020**, *168*, 448–457. [CrossRef]
94. Matthews, P.D.; King, T.C.; Glass, H.; Magusin, P.C.M.M.; Tustin, G.J.; Brown, P.A.C.; Cormack, J.A.; García-Rodríguez, R.; Leskes, M.; Dutton, S.E.; et al. Synthesis and Extensive Characterisation of Phosphorus Doped Graphite. *RSC Adv.* **2016**, *6*, 62140–62145. [CrossRef]
95. Groult, H.; Nakajima, T.; Perrigaud, L.; Ohzawa, Y.; Yashiro, H.; Komaba, S.; Kumagai, N. Surface-Fluorinated Graphite Anode Materials for Li-Ion Batteries. *J. Fluor. Chem.* **2005**, *126*, 1111–1116. [CrossRef]
96. Divya, M.L.; Natarajan, S.; Aravindan, V. Graphene from Spent Lithium-Ion Batteries. *Batter. Supercaps* **2022**, *5*, e202200046. [CrossRef]
97. Li, Y.; Guo, W.; Stroe, D.-I.; Zhao, H.; Kjær Kristensen, P.; Rosgaard Jensen, L.; Pedersen, K.; Gurevich, L. Evolution of Aging Mechanisms and Performance Degradation of Lithium-Ion Battery from Moderate to Severe Capacity Loss Scenarios. *Chem. Eng. J.* **2024**, *498*, 155588. [CrossRef]
98. Synthetic versus Natural Graphite Debate Rages on: 2023 Preview. Available online: <https://www.fastmarkets.com/insights/synthetic-versus-natural-graphite-debate/#:~:text=Total%20apparent%20demand%20for%20natural,1.28%20million%20tonnes%20in%202022> (accessed on 20 February 2025).
99. Pérez, B.; Echeberria, J. Influence of Abrasives and Graphite on Processing and Properties of Sintered Metallic Friction Materials. *Heliyon* **2019**, *5*, e02311. [CrossRef] [PubMed]
100. Park, J.; Xu, Z.-L.; Kang, K. Solvated Ion Intercalation in Graphite: Sodium and Beyond. *Front. Chem.* **2020**, *8*, 432. [CrossRef]
101. Niu, S.; Zhu, G.; Wu, K.; Zheng, H. The Feasibility for Natural Graphite to Replace Artificial Graphite in Organic Electrolyte with Different Film-Forming Additives. *Chin. J. Chem. Eng.* **2023**, *56*, 58–69. [CrossRef]
102. Erickson, E.M.; Markevich, E.; Salitra, G.; Sharon, D.; Hirshberg, D.; De La Llave, E.; Shterenberg, I.; Rosenman, A.; Frimer, A.; Aurbach, D. Review—Development of Advanced Rechargeable Batteries: A Continuous Challenge in the Choice of Suitable Electrolyte Solutions. *J. Electrochem. Soc.* **2015**, *162*, A2424–A2438. [CrossRef]
103. Rey, I.; Vallejo, C.; Santiago, G.; Iturrondobeitia, M.; Lizundia, E. Environmental Impacts of Graphite Recycling from Spent Lithium-Ion Batteries Based on Life Cycle Assessment. *ACS Sustain. Chem. Eng.* **2021**, *9*, 14488–14501. [CrossRef]
104. Zhang, J.; Liang, C.; Dunn, J.B. Graphite Flows in the U.S.: Insights into a Key Ingredient of Energy Transition. *Environ. Sci. Technol.* **2023**, *57*, 3402–3414. [CrossRef]
105. Esteve-Adell, I.; Porcel-Valenzuela, M.; Zubizarreta, L.; Gil-Agustí, M.; García-Pellicer, M.; Quijano-Lopez, A. Influence of the Specific Surface Area of Graphene Nanoplatelets on the Capacity of Lithium-Ion Batteries. *Front. Chem.* **2022**, *10*, 807980. [CrossRef]
106. Liu, Z.; Shi, Y.; Yang, Q.; Shen, H.; Fan, Q.; Nie, H. Effects of Crystal Structure and Electronic Properties on Lithium Storage Performance of Artificial Graphite. *RSC Adv.* **2023**, *13*, 29923–29930. [CrossRef]
107. Pati, S.K.; Hwang, Y.; Lee, H.-M.; Kim, B.-J.; Park, S. Porous Activated Carbon Derived from Petroleum Coke as a High-Performance Anodic Electrode Material for Supercapacitors. *Carbon Lett.* **2024**, *34*, 153–162. [CrossRef]
108. Yue, J.; Zhu, Y.; Lv, J.; Wang, Y.; Cheng, J.; Zhao, X. Application and Research Progress of Coating Pitch in Anode Materials for Lithium-Ion Batteries. *Chem. Eng. Sci.* **2024**, *297*, 120302. [CrossRef]
109. Liang, C.; Chen, Y.; Wu, M.; Wang, K.; Zhang, W.; Gan, Y.; Huang, H.; Chen, J.; Xia, Y.; Zhang, J.; et al. Green Synthesis of Graphite from CO₂ Without Graphitization Process of Amorphous Carbon. *Nat. Commun.* **2021**, *12*, 119. [CrossRef] [PubMed]
110. Kamal, A.S.; Othman, R.; Jabarullah, N.H. Preparation and Synthesis of Synthetic Graphite from Biomass Waste: A Review. *Syst. Rev. Pharm.* **2020**, *11*, 881–894.
111. Eftekhari, A. Lithium-Ion Batteries with High Rate Capabilities. *ACS Sustain. Chem. Eng.* **2017**, *5*, 2799–2816. [CrossRef]
112. Li, Y.; Fan, Z.; Li, S.; Zhao, Y.; Li, Z.; Xu, C.; Dou, H.; Zhang, X. A Successive Intercalation–Deposition Mechanism Induced by Hard Carbon for Hybrid Lithium-Ion/Lithium Metal Batteries. *J. Energy Chem.* **2025**, *in press*. [CrossRef]

113. Xu, X.; Han, X.; Lu, L.; Wang, F.; Yang, M.; Liu, X.; Wu, Y.; Tang, S.; Hou, Y.; Hou, J.; et al. Challenges and Opportunities Toward Long-Life Lithium-Ion Batteries. *J. Power Sources* **2024**, *603*, 234445. [[CrossRef](#)]
114. Yang, C.; Jiang, Z.; Chen, X.; Luo, W.; Zhou, T.; Yang, J. Lithium Metal Based Battery Systems with Ultra-High Energy Density Beyond 500 W h Kg⁻¹. *Chem. Commun.* **2024**, *60*, 10245–10264. [[CrossRef](#)]
115. Placke, T.; Kloepsch, R.; Dühnen, S.; Winter, M. Lithium Ion, Lithium Metal, and Alternative Rechargeable Battery Technologies: The Odyssey for High Energy Density. *J. Solid State Electrochem.* **2017**, *21*, 1939–1964. [[CrossRef](#)]
116. IEA. *Energy Technology Perspectives 2023*; IEA: Paris, France, 2023.
117. Hofmann, U.; Rüdorff, W. The Formation of Salts from Graphite by Strong Acids. *Trans. Faraday Soc.* **1938**, *34*, 1017–1021. [[CrossRef](#)]
118. Besenhard, J.O. The Electrochemical Preparation and Properties of Ionic Alkali Metal-and NR4-Graphite Intercalation Compounds in Organic Electrolytes. *Carbon* **1976**, *14*, 111–115. [[CrossRef](#)]
119. Rüdorff, W.; Stumpf, E.; Spriessler, W.; Siecke, F.W. Reactions of Graphite with Metal Chlorides. *Angew. Chem. Int. Ed. Engl.* **1963**, *2*, 67–73. [[CrossRef](#)]
120. Oka, H.; Makimura, Y.; Uyama, T.; Nonaka, T.; Kondo, Y.; Okuda, C. Changes in the Stage Structure of Li-Intercalated Graphite Electrode at Elevated Temperatures. *J. Power Sources* **2021**, *482*, 228926. [[CrossRef](#)]
121. Gavilán-Arriazu, E.M.; Pinto, O.A.; López De Mishima, B.A.; Barraco, D.E.; Oviedo, O.A.; Leiva, E.P.M. The Kinetic Origin of the Daumas-Hérolé Model for the Li-Ion/Graphite Intercalation System. *Electrochem. Commun.* **2018**, *93*, 133–137. [[CrossRef](#)]
122. Yoda, S.; Ishihara, K. The Advent of Battery-Based Societies and the Global Environment in the 21st Century. *J. Power Sources* **1999**, *81*–82, 162–169. [[CrossRef](#)]
123. Edge, J.S.; O’Kane, S.; Prosser, R.; Kirkaldy, N.D.; Patel, A.N.; Hales, A.; Ghosh, A.; Ai, W.; Chen, J.; Yang, J.; et al. Lithium Ion Battery Degradation: What You Need to Know. *Phys. Chem. Chem. Phys.* **2021**, *23*, 8200–8221. [[CrossRef](#)]
124. Wright, R.B.; Motloch, C.G.; Belt, J.R.; Christophersen, J.P.; Ho, C.D.; Richardson, R.A.; Bloom, I.; Jones, S.A.; Battaglia, V.S.; Henriksen, G.L.; et al. Calendar- and Cycle-Life Studies of Advanced Technology Development Program Generation 1 Lithium-Ion Batteries. *J. Power Sources* **2002**, *110*, 445–470. [[CrossRef](#)]
125. De Hoog, J.; Timmermans, J.-M.; Ioan-Stroe, D.; Swierczynski, M.; Jaguemont, J.; Goutam, S.; Omar, N.; Van Mierlo, J.; Van Den Bossche, P. Combined Cycling and Calendar Capacity Fade Modeling of a Nickel-Manganese-Cobalt Oxide Cell with Real-Life Profile Validation. *Appl. Energy* **2017**, *200*, 47–61. [[CrossRef](#)]
126. Feinauer, M.; Wohlfahrt-Mehrens, M.; Hölzle, M.; Waldmann, T. Temperature-Driven Path Dependence in Li-Ion Battery Cyclic Aging. *J. Power Sources* **2024**, *594*, 233948. [[CrossRef](#)]
127. Liu, Q.; Rao, A.M.; Han, X.; Lu, B. Artificial SEI for Superhigh-Performance K-Graphite Anode. *Adv. Sci.* **2021**, *8*, 2003639. [[CrossRef](#)]
128. Tzeng, Y.; Jhan, C.-Y.; Sung, S.-H.; Chiou, Y.-Y. Effects of Crystalline Diamond Nanoparticles on Silicon Thin Films as an Anode for a Lithium-Ion Battery. *Batteries* **2024**, *10*, 321. [[CrossRef](#)]
129. Sagar, R.U.R.; Mahmood, N.; Stadler, F.J.; Anwar, T.; Navale, S.T.; Shehzad, K.; Du, B. High Capacity Retention Anode Material for Lithium Ion Battery. *Electrochim. Acta* **2016**, *211*, 156–163. [[CrossRef](#)]
130. Liang, B.; Liu, Y.; Xu, Y. Silicon-Based Materials as High Capacity Anodes for Next Generation Lithium Ion Batteries. *J. Power Sources* **2014**, *267*, 469–490. [[CrossRef](#)]
131. Song, T.; Jeon, Y.; Paik, U. Si Nanotubes Array Sheathed with SiN/SiOxNy Layer as an Anode Material for Lithium Ion Batteries. *J. Electroceramics* **2014**, *32*, 66–71. [[CrossRef](#)]
132. Shen, Y.; Qian, J.; Yang, H.; Zhong, F.; Ai, X. Chemically Prelithiated Hard-Carbon Anode for High Power and High Capacity Li-Ion Batteries. *Small* **2020**, *16*, 1907602. [[CrossRef](#)]
133. Liu, Y.; Li, X.; Guo, H.; Wang, Z.; Peng, W.; Yang, Y.; Liang, R. Effect of Carbon Nanotube on the Electrochemical Performance of C-LiFePO₄/Graphite Battery. *J. Power Sources* **2008**, *184*, 522–526. [[CrossRef](#)]
134. An, S.J.; Li, J.; Daniel, C.; Mohanty, D.; Nagpure, S.; Wood, D.L. The State of Understanding of the Lithium-Ion-Battery Graphite Solid Electrolyte Interphase (SEI) and Its Relationship to Formation Cycling. *Carbon* **2016**, *105*, 52–76. [[CrossRef](#)]
135. Blomgren, G.E. Liquid Electrolytes for Lithium and Lithium-Ion Batteries. *J. Power Sources* **2003**, *119*–121, 326–329. [[CrossRef](#)]
136. Huang, Y.; Yang, H.; Gao, Y.; Chen, G.; Li, Y.; Shi, L.; Zhang, D. Mechanism and Solutions of Lithium Dendrite Growth in Lithium Metal Batteries. *Mater. Chem. Front.* **2024**, *8*, 1282–1299. [[CrossRef](#)]
137. Ong, M.T.; Verners, O.; Draeger, E.W.; Van Duin, A.C.T.; Lordi, V.; Pask, J.E. Lithium Ion Solvation and Diffusion in Bulk Organic Electrolytes from First-Principles and Classical Reactive Molecular Dynamics. *J. Phys. Chem. B* **2015**, *119*, 1535–1545. [[CrossRef](#)]
138. Li, S.; Luo, Z.; Li, L.; Hu, J.; Zou, G.; Hou, H.; Ji, X. Recent Progress on Electrolyte Additives for Stable Lithium Metal Anode. *Energy Storage Mater.* **2020**, *32*, 306–319. [[CrossRef](#)]
139. Dou, F.; Shi, L.; Chen, G.; Zhang, D. Silicon/Carbon Composite Anode Materials for Lithium-Ion Batteries. *Electrochem. Energy Rev.* **2019**, *2*, 149–198. [[CrossRef](#)]

140. Mei, Y.; He, Y.; Zhu, H.; Ma, Z.; Pu, Y.; Chen, Z.; Li, P.; He, L.; Wang, W.; Tang, H. Recent Advances in the Structural Design of Silicon/Carbon Anodes for Lithium Ion Batteries: A Review. *Coatings* **2023**, *13*, 436. [[CrossRef](#)]
141. Yang, Z.; Shen, J.; Archer, L.A. An In Situ Method of Creating Metal Oxide–Carbon Composites and Their Application as Anode Materials for Lithium-Ion Batteries. *J. Mater. Chem.* **2011**, *21*, 11092. [[CrossRef](#)]
142. Putois, F. Market for Nickel-Cadmium Batteries. *J. Power Sources* **1995**, *57*, 67–70. [[CrossRef](#)]
143. Nishi, Y. Lithium Ion Secondary Batteries; Past 10 Years and the Future. *J. Power Sources* **2001**, *100*, 101–106. [[CrossRef](#)]
144. De, S.; Northrop, P.W.C.; Ramadesigan, V.; Subramanian, V.R. Model-Based Simultaneous Optimization of Multiple Design Parameters for Lithium-Ion Batteries for Maximization of Energy Density. *J. Power Sources* **2013**, *227*, 161–170. [[CrossRef](#)]
145. Goodenough, J.B.; Kim, Y. Challenges for Rechargeable Li Batteries. *Chem. Mater.* **2010**, *22*, 587–603. [[CrossRef](#)]
146. Goriparti, S.; Miele, E.; De Angelis, F.; Di Fabrizio, E.; Proietti Zaccaria, R.; Capiglia, C. Review on Recent Progress of Nanostructured Anode Materials for Li-Ion Batteries. *J. Power Sources* **2014**, *257*, 421–443. [[CrossRef](#)]
147. Wang, Z.; Zhang, Y.; Zhang, B.; Yang, D.; Zhou, K.; Huang, Y.; Wang, F.; Duan, J.; Wang, X.; Dong, P.; et al. Enhanced Electrochemical Performance of a Cost-Effective Sm_2O_3 -Coated Spinel $\text{LiNi}_{0.5}\text{Mn}_{1.5}\text{O}_4$ Cathode for High-Voltage Lithium-Ion Batteries. *J. Power Sources* **2024**, *614*, 235008. [[CrossRef](#)]
148. Zhu, C.; Shen, X.; Gao, Z.; Li, Y.; Wu, X.; Zhao, J.; Zhou, P.; Zhuo, S.; Zhou, J. Enhancing Electrochemical Performance of Fluorinated Graphite by Polydopamine–Derived Nitrogen–Doped Carbon Coating. *Electrochim. Acta* **2022**, *425*, 140718. [[CrossRef](#)]
149. Wang, F.; Lin, S.; Lu, X.; Hong, R.; Liu, H. Poly-Dopamine Carbon-Coated Stable Silicon/Graphene/CNT Composite as Anode for Lithium Ion Batteries. *Electrochim. Acta* **2022**, *404*, 139708. [[CrossRef](#)]
150. Liu, P.; Peng, J.; He, L.; Yang, J.; Tang, Y.; Zhou, K.; Xie, Z.; Wang, X. Amorphous Carbon Coating Enabling Waste Graphite to Reuse as High-Performance Anode of Lithium-Ion Battery. *ACS Appl. Energy Mater.* **2025**, *8*, 442–451. [[CrossRef](#)]
151. Hafiz, W.; Du, B.; Zhang, J.; Xiao, M.; Meng, Y.; Zhu, F. Enhancing the Performance of Lithium-Ion Batteries with $\text{NiCo}_2\text{S}_4/\text{C}$ -Hollow Sphere Nanocomposites. *J. Mater. Sci. Mater. Electron.* **2024**, *35*, 1987. [[CrossRef](#)]
152. Asasian-Kolur, N.; Sharifian, S.; Haddadi, B.; Jordan, C.; Harasek, M. Ordered Porous Carbon Preparation by Hard Templating Approach for Hydrogen Adsorption Application. *Biomass Convers. Biorefinery* **2024**, *14*, 18381–18416. [[CrossRef](#)]
153. Li, Z.; Ottmann, A.; Zhang, T.; Sun, Q.; Meyer, H.-P.; Vaynzof, Y.; Xiang, J.; Klingeler, R. Preparation of Hierarchical $\text{C@MoS}_2 @\text{C}$ Sandwiched Hollow Spheres for Lithium Ion Batteries. *J. Mater. Chem. A* **2017**, *5*, 3987–3994. [[CrossRef](#)]
154. Chuenchom, L.; Krahnert, R.; Smarsly, B.M. Recent Progress in Soft-Templating of Porous Carbon Materials. *Soft Matter* **2012**, *8*, 10801. [[CrossRef](#)]
155. Li, C.; Li, Q.; Kaneti, Y.V.; Hou, D.; Yamauchi, Y.; Mai, Y. Self-Assembly of Block Copolymers Towards Mesoporous Materials for Energy Storage and Conversion Systems. *Chem. Soc. Rev.* **2020**, *49*, 4681–4736. [[CrossRef](#)]
156. Feyzi, E.; Madikere Raghunatha Reddy, A.K.; Li, X.; Deng, S.; Nanda, J.; Zaghib, K. A Comprehensive Review of Silicon Anodes for High-Energy Lithium-Ion Batteries: Challenges, Latest Developments, and Perspectives. *Energy* **2024**, *5*, 100176. [[CrossRef](#)]
157. Ji, H.; Xu, X.; Li, X.; Li, K.; Yuan, L.; Han, Z.; Tang, K. A Low-Cost Si@C Composite for Lithium-Ion Batteries Anode Materials Synthesized via Freeze-Drying Process Using Kerf Loss Si Waste. *Ionics* **2024**, *30*, 2585–2599. [[CrossRef](#)]
158. Poetke, S.; Hippauf, F.; Baasner, A.; Dörfler, S.; Althues, H.; Kaskel, S. Nanostructured Si–C Composites as High-Capacity Anode Material for All-Solid-State Lithium-Ion Batteries. *Batter. Supercaps* **2021**, *4*, 1323–1334. [[CrossRef](#)]
159. Park, I.; Lee, H.; Chae, O.B. Synthesis Methods of Si/C Composite Materials for Lithium-Ion Batteries. *Batteries* **2024**, *10*, 381. [[CrossRef](#)]
160. Xin, F.; Whittingham, M.S. Challenges and Development of Tin-Based Anode with High Volumetric Capacity for Li-Ion Batteries. *Electrochim. Energy Rev.* **2020**, *3*, 643–655. [[CrossRef](#)]
161. Fang, G.; Liu, W.; Kaneko, S.; Xia, B.; Sun, H.; Zheng, J.; Li, D. Preparation, Microstructure, and Electrochemical Properties of Sn-Co-C Anode Materials Using Composited Carbon Sources. *J. Solid State Electrochem.* **2013**, *17*, 2521–2529. [[CrossRef](#)]
162. Zheng, H.; Qu, Q.; Zhang, L.; Liu, G.; Battaglia, V.S. Hard Carbon: A Promising Lithium-Ion Battery Anode for High Temperature Applications with Ionic Electrolyte. *RSC Adv.* **2012**, *2*, 4904. [[CrossRef](#)]
163. Matsunaga, T.; Takagi, S.; Shimoda, K.; Okazaki, K.; Ishikawa, Y.; Yonemura, M.; Ukyo, Y.; Fukunaga, T.; Matsubara, E. Comprehensive Elucidation of Crystal Structures of Lithium-Intercalated Graphite. *Carbon* **2019**, *142*, 513–517. [[CrossRef](#)]
164. Liu, X.; Si, Y.; Li, K.; Xu, Y.; Zhao, Z.; Li, C.; Fu, Y.; Li, D. Exploring Sodium Storage Mechanism of Topological Insulator Bi_2Te_3 Nanosheets Encapsulated in Conductive Polymer. *Energy Storage Mater.* **2021**, *41*, 255–263. [[CrossRef](#)]
165. Park, S.-H.; Kim, H.J.; Lee, J.; Jeong, Y.K.; Choi, J.W.; Lee, H. Mussel-Inspired Polydopamine Coating for Enhanced Thermal Stability and Rate Performance of Graphite Anodes in Li-Ion Batteries. *ACS Appl. Mater. Interfaces* **2016**, *8*, 13973–13981. [[CrossRef](#)]
166. Du, J.; Wang, W.; Jia, H.; Li, T.; Song, K. High-Rate Soft Carbon Anode for Lithium Storage: From Modified Pitch Molecular Structure to Ordered Carbon Microcrystals. *Ionics* **2024**, *31*, 151–163. [[CrossRef](#)]
167. Zuo, X.; Zhu, J.; Müller-Buschbaum, P.; Cheng, Y.-J. Silicon Based Lithium-Ion Battery Anodes: A Chronicle Perspective Review. *Nano Energy* **2017**, *31*, 113–143. [[CrossRef](#)]

168. Wang, L.; Zhang, X.; Yan, F.; Chan, H.L.W.; Ding, F. Mechanism of Boron and Nitrogen In Situ Doping during Graphene Chemical Vapor Deposition Growth. *Carbon* **2016**, *98*, 633–637. [CrossRef]
169. Daigle, J.-C.; Baray, F.; Gagnon, C.; Clément, D.; Hovington, P.; Demers, H.; Guerfi, A.; Zaghib, K. Amphiphilic Latex as a Water-Based Binder for LiFePO₄ Cathode. *J. Power Sources* **2019**, *415*, 172–178. [CrossRef]
170. Chitrainingrum, N.; Gunawan, F.; Farma, R.; Subyakto, S.; Subhan, A.; Fudholi, A.; Rajani, A.; Apriyani, I.; Manurung, K.S.; Ramadhan, F.A.; et al. Nitrogen-Doped Activated Carbon Derived from Oil Palm Empty Fruit Bunch (OPEFB) for Sustainable Lithium-Ion Battery. *Biomass Convers. Biorefinery* **2024**. [CrossRef]
171. Geng, H.; Zhou, Q.; Pan, Y.; Gu, H.; Zheng, J. Preparation of Fluorine-Doped, Carbon-Encapsulated Hollow Fe₃O₄ Spheres as an Efficient Anode Material for Li-Ion Batteries. *Nanoscale* **2014**, *6*, 3889. [CrossRef] [PubMed]
172. Wang, H.; Zhang, C.; Liu, Z.; Wang, L.; Han, P.; Xu, H.; Zhang, K.; Dong, S.; Yao, J.; Cui, G. Nitrogen-Doped Graphene Nanosheets with Excellent Lithium Storage Properties. *J. Mater. Chem.* **2011**, *21*, 5430. [CrossRef]
173. Kim, K.-J.; Lee, T.-S.; Kim, H.-G.; Lim, S.-H.; Lee, S.-M. A Hard Carbon/Microcrystalline Graphite/Carbon Composite with a Core-Shell Structure as Novel Anode Materials for Lithium-Ion Batteries. *Electrochim. Acta* **2014**, *135*, 27–34. [CrossRef]
174. Rodríguez, E.; Cameán, I.; García, R.; García, A.B. Graphitized Boron-Doped Carbon Foams: Performance as Anodes in Lithium-Ion Batteries. *Electrochim. Acta* **2011**, *56*, 5090–5094. [CrossRef]
175. Wang, C.; Zhao, H.; Wang, J.; Wang, J.; Lv, P. Electrochemical Performance of Modified Artificial Graphite as Anode Material for Lithium Ion Batteries. *Ionics* **2013**, *19*, 221–226. [CrossRef]
176. Xu, J.-L.; Zhang, X.; Miao, Y.-X.; Wen, M.-X.; Yan, W.-J.; Lu, P.; Wang, Z.-R.; Sun, Q. In-Situ Plantation of Fe₃O₄@C Nanoparticles on Reduced Graphene Oxide Nanosheet as High-Performance Anode for Lithium/Sodium-Ion Batteries. *Appl. Surf. Sci.* **2021**, *546*, 149163. [CrossRef]
177. Feng, T.; Xu, Y.; Zhang, Z.; Du, X.; Sun, X.; Xiong, L.; Rodriguez, R.; Holze, R. Low-Cost Al₂O₃ Coating Layer As a Preformed SEI on Natural Graphite Powder To Improve Coulombic Efficiency and High-Rate Cycling Stability of Lithium-Ion Batteries. *ACS Appl. Mater. Interfaces* **2016**, *8*, 6512–6519. [CrossRef]
178. Cui, Z.; Wang, L.; Li, Q.; Wang, K. A Comprehensive Review on the State of Charge Estimation for Lithium-Ion Battery Based on Neural Network. *Int. J. Energy Res.* **2022**, *46*, 5423–5440. [CrossRef]
179. Lee, S.; Kim, J.; Lee, J.; Cho, B.H. State-of-Charge and Capacity Estimation of Lithium-Ion Battery Using a New Open-Circuit Voltage Versus State-of-Charge. *J. Power Sources* **2008**, *185*, 1367–1373. [CrossRef]
180. Wang, Y.; Zhao, L.; Cheng, J.; Zhou, J.; Wang, S. A State of Charge Estimation Method of Lithium-Ion Battery Based on Fused Open Circuit Voltage Curve. *Appl. Sci.* **2020**, *10*, 1264. [CrossRef]
181. Dahn, J.R.; Zheng, T.; Liu, Y.; Xue, J.S. Mechanisms for Lithium Insertion in Carbonaceous Materials. *Science* **1995**, *270*, 590–593. [CrossRef]
182. Stevens, D.A.; Dahn, J.R. High Capacity Anode Materials for Rechargeable Sodium-Ion Batteries. *J. Electrochem. Soc.* **2000**, *147*, 1271. [CrossRef]
183. Lou, T.T.; Zhang, W.G.; Guo, H.Y.; Wang, J.S. The Internal Resistance Characteristics of Lithium-Ion Battery Based on HPPC Method. *Adv. Mater. Res.* **2012**, *455–456*, 246–251. [CrossRef]
184. Stolz, L.; Winter, M.; Kasnatscheew, J. Practical Relevance of Charge Transfer Resistance at the Li Metal Electrode | electrolyte Interface in Batteries? *J. Solid State Electrochem.* **2024**. [CrossRef]
185. Wang, X.; Wei, X.; Dai, H. Estimation of State of Health of Lithium-Ion Batteries Based on Charge Transfer Resistance Considering Different Temperature and State of Charge. *J. Energy Storage* **2019**, *21*, 618–631. [CrossRef]
186. Eom, K.; Jung, J.; Lee, J.T.; Lair, V.; Joshi, T.; Lee, S.W.; Lin, Z.; Fuller, T.F. Improved Stability of Nano-Sn Electrode with High-Quality Nano-SEI Formation for Lithium Ion Battery. *Nano Energy* **2015**, *12*, 314–321. [CrossRef]
187. Huang, Q.-A.; Shen, Y.; Huang, Y.; Zhang, L.; Zhang, J. Impedance Characteristics and Diagnoses of Automotive Lithium-Ion Batteries at 7.5% to 93.0% State of Charge. *Electrochim. Acta* **2016**, *219*, 751–765. [CrossRef]
188. Ruggeri, I.; Martin, J.; Wohlfahrt-Mehrens, M.; Mancini, M. Interfacial Kinetics and Low-Temperature Behavior of Spheroidized Natural Graphite Particles as Anode for Li-Ion Batteries. *J. Solid State Electrochem.* **2022**, *26*, 73–83. [CrossRef]
189. Nam, K.-H.; Hwa Chae, K.; Choi, J.-H.; Jeon, K.-J.; Park, C.-M. Superior Carbon Black: High-Performance Anode and Conducting Additive for Rechargeable Li- and Na-Ion Batteries. *Chem. Eng. J.* **2021**, *417*, 129242. [CrossRef]
190. Kong, L.; Li, Y.; Feng, W. Strategies to Solve Lithium Battery Thermal Runaway: From Mechanism to Modification. *Electrochem. Energy Rev.* **2021**, *4*, 633–679. [CrossRef]
191. Abraham, D.P.; Roth, E.P.; Kostecki, R.; McCarthy, K.; MacLaren, S.; Doughty, D.H. Diagnostic Examination of Thermally Abused High-Power Lithium-Ion Cells. *J. Power Sources* **2006**, *161*, 648–657. [CrossRef]
192. Klein, E.J.; Carter, R.; Love, C.T. Accelerating Rate Calorimetry and Complementary Techniques to Characterize Battery Safety Hazards. *J. Vis. Exp.* **2021**, *15*, 60342. [CrossRef] [PubMed]
193. Md Said, M.S.; Mohd Tohir, M.Z. Characterisation of Thermal Runaway Behaviour of Cylindrical Lithium-Ion Battery Using Accelerating Rate Calorimeter and Oven Heating. *Case Stud. Therm. Eng.* **2021**, *28*, 101474. [CrossRef]

194. Yang, Y.; Chen, L.; Yang, L.; Du, X.; Yang, Y. Capacity Fade Characteristics of Lithium Iron Phosphate Cell during Dynamic Cycle. *Energy* **2020**, *206*, 118155. [[CrossRef](#)]
195. Fan, J.; Tan, S. Studies on Charging Lithium-Ion Cells at Low Temperatures. *J. Electrochem. Soc.* **2006**, *153*, A1081. [[CrossRef](#)]
196. Hausbrand, R.; Cherkashinin, G.; Ehrenberg, H.; Grötting, M.; Albe, K.; Hess, C.; Jaegermann, W. Fundamental Degradation Mechanisms of Layered Oxide Li-Ion Battery Cathode Materials: Methodology, Insights and Novel Approaches. *Mater. Sci. Eng. B* **2015**, *192*, 3–25. [[CrossRef](#)]
197. Sharifi-Asl, S.; Lu, J.; Amine, K.; Shahbazian-Yassar, R. Oxygen Release Degradation in Li-Ion Battery Cathode Materials: Mechanisms and Mitigating Approaches. *Adv. Energy Mater.* **2019**, *9*, 1900551. [[CrossRef](#)]
198. Kalnaus, S.; Wang, Y.; Turner, J.A. Mechanical Behavior and Failure Mechanisms of Li-Ion Battery Separators. *J. Power Sources* **2017**, *348*, 255–263. [[CrossRef](#)]
199. Larsson, F.; Mellander, B.-E. Abuse by External Heating, Overcharge and Short Circuiting of Commercial Lithium-Ion Battery Cells. *J. Electrochem. Soc.* **2014**, *161*, A1611–A1617. [[CrossRef](#)]
200. Lai, X.; Jin, C.; Yi, W.; Han, X.; Feng, X.; Zheng, Y.; Ouyang, M. Mechanism, Modeling, Detection, and Prevention of the Internal Short Circuit in Lithium-Ion Batteries: Recent Advances and Perspectives. *Energy Storage Mater.* **2021**, *35*, 470–499. [[CrossRef](#)]
201. Saito, Y.; Takano, K.; Negishi, A. Thermal Behaviors of Lithium-Ion Cells during Overcharge. *J. Power Sources* **2001**, *97–98*, 693–696. [[CrossRef](#)]
202. Yuge, R.; Tamura, N.; Manako, T.; Nakano, K.; Nakahara, K. High-Rate Charge/Discharge Properties of Li-Ion Battery Using Carbon-Coated Composites of Graphites, Vapor Grown Carbon Fibers, and Carbon Nanohorns. *J. Power Sources* **2014**, *266*, 471–474. [[CrossRef](#)]
203. Jung, Y.S.; Cavanagh, A.S.; Riley, L.A.; Kang, S.; Dillon, A.C.; Groner, M.D.; George, S.M.; Lee, S. Ultrathin Direct Atomic Layer Deposition on Composite Electrodes for Highly Durable and Safe Li-Ion Batteries. *Adv. Mater.* **2010**, *22*, 2172–2176. [[CrossRef](#)] [[PubMed](#)]
204. Xu, T.; Zhou, C.; Zhou, H.; Wang, Z.; Ren, J. Synthesis of Alumina-Coated Natural Graphite for Highly Cycling Stability and Safety of Li-Ion Batteries. *Chin. J. Chem.* **2019**, *37*, 342–346. [[CrossRef](#)]
205. Wang, Z.; Wang, L.; Zhang, H.; Xu, H.; He, X. Materials Descriptors of Machine Learning to Boost Development of Lithium-Ion Batteries. *Nano Converg.* **2024**, *11*, 8. [[CrossRef](#)]
206. Ghodake, A.; Sadakale, R.; Dhanvijay, M.; Mandhana, A.; Joshi, U. Integrating Thermal Mechanisms with Machine Learning for Accurate State of Health Estimation in Lithium-Ion Batteries. In *Proceedings of the 12th International Conference on Soft Computing for Problem Solving*; Pant, M., Deep, K., Nagar, A., Eds.; Lecture Notes in Networks and Systems; Springer Nature: Singapore, 2024; Volume 994, pp. 767–782, ISBN 978-981-97-3179-4.
207. Valizadeh, A.; Amirhosseini, M.H. Machine Learning in Lithium-Ion Battery: Applications, Challenges, and Future Trends. *SN Comput. Sci.* **2024**, *5*, 717. [[CrossRef](#)]
208. Darga, J.; Lamb, J.; Manthiram, A. Industrialization of Layered Oxide Cathodes for Lithium-Ion and Sodium-Ion Batteries: A Comparative Perspective. *Energy Technol.* **2020**, *8*, 2000723. [[CrossRef](#)]
209. Wu, H.; Hao, J.; Jiang, Y.; Jiao, Y.; Liu, J.; Xu, X.; Davey, K.; Wang, C.; Qiao, S.-Z. Alkaline-Based Aqueous Sodium-Ion Batteries for Large-Scale Energy Storage. *Nat. Commun.* **2024**, *15*, 575. [[CrossRef](#)]
210. Li, Y.; Lu, Y.; Zhao, C.; Hu, Y.-S.; Titirici, M.-M.; Li, H.; Huang, X.; Chen, L. Recent Advances of Electrode Materials for Low-Cost Sodium-Ion Batteries towards Practical Application for Grid Energy Storage. *Energy Storage Mater.* **2017**, *7*, 130–151. [[CrossRef](#)]
211. Chang, X.; Yang, Z.; Liu, Y.; Chen, J.; Wu, M.; Li, L.; Chou, S.; Qiao, Y. The Guarantee of Large-Scale Energy Storage: Non-Flammable Organic Liquid Electrolytes for High-Safety Sodium Ion Batteries. *Energy Storage Mater.* **2024**, *69*, 103407. [[CrossRef](#)]
212. Nobuhara, K.; Nakayama, H.; Nose, M.; Nakanishi, S.; Iba, H. First-Principles Study of Alkali Metal-Graphite Intercalation Compounds. *J. Power Sources* **2013**, *243*, 585–587. [[CrossRef](#)]
213. Lyu, L.; Yi, Y.; Xu, Z. Graphite Co-Intercalation Chemistry in Sodium-Ion Batteries. *Batter. Supercaps* **2024**, *8*, e202400521. [[CrossRef](#)]
214. Liu, Y.; Merinov, B.V.; Goddard, W.A. Origin of Low Sodium Capacity in Graphite and Generally Weak Substrate Binding of Na and Mg Among Alkali and Alkaline Earth Metals. *Proc. Natl. Acad. Sci. USA* **2016**, *113*, 3735–3739. [[CrossRef](#)] [[PubMed](#)]
215. Jache, B.; Adelhelm, P. Use of Graphite as a Highly Reversible Electrode with Superior Cycle Life for Sodium-Ion Batteries by Making Use of Co-Intercalation Phenomena. *Angew. Chem. Int. Ed.* **2014**, *53*, 10169–10173. [[CrossRef](#)] [[PubMed](#)]
216. Kim, H.; Kim, H.; Ding, Z.; Lee, M.H.; Lim, K.; Yoon, G.; Kang, K. Recent Progress in Electrode Materials for Sodium-Ion Batteries. *Adv. Energy Mater.* **2016**, *6*, 1600943. [[CrossRef](#)]
217. Kim, H.; Hong, J.; Yoon, G.; Kim, H.; Park, K.-Y.; Park, M.-S.; Yoon, W.-S.; Kang, K. Sodium Intercalation Chemistry in Graphite. *Energy Environ. Sci.* **2015**, *8*, 2963–2969. [[CrossRef](#)]
218. Jache, B.; Binder, J.O.; Abe, T.; Adelhelm, P. A Comparative Study on the Impact of Different Glymes and Their Derivatives as Electrolyte Solvents for Graphite Co-Intercalation Electrodes in Lithium-Ion and Sodium-Ion Batteries. *Phys. Chem. Chem. Phys.* **2016**, *18*, 14299–14316. [[CrossRef](#)]

219. Escher, I.; Freytag, A.I.; López Del Amo, J.M.; Adelhelm, P. Solid-State NMR Study on the Structure and Dynamics of Graphite Electrodes in Sodium-Ion Batteries with Solvent Co-Intercalation. *Batter. Supercaps* **2023**, *6*, e202200421. [CrossRef]
220. Chen, Y.; Zhang, S.; Zhang, W.; Quadrelli, A.; Jarvis, S.; Chen, J.; Lu, H.; Mangayarkarasi, N.; Niu, Y.; Tao, J.; et al. Operando Nano-Mapping of Sodium-Diglyme Co-Intercalation and SEI Formation in Sodium Ion Batteries’ Graphene Anodes. *Appl. Phys. Rev.* **2024**, *11*, 021422. [CrossRef]
221. Maibach, J.; Jeschull, F.; Brandell, D.; Edström, K.; Valvo, M. Surface Layer Evolution on Graphite During Electrochemical Sodium-Tetraglyme Co-Intercalation. *ACS Appl. Mater. Interfaces* **2017**, *9*, 12373–12381. [CrossRef] [PubMed]
222. Hofmann, A.; Wang, Z.; Bautista, S.P.; Weil, M.; Müller, F.; Löwe, R.; Schneider, L.; Mohsin, I.U.; Hanemann, T. Comprehensive Characterization of Propylene Carbonate Based Liquid Electrolyte Mixtures for Sodium-Ion Cells. *Electrochim. Acta* **2022**, *403*, 139670. [CrossRef]
223. Parveen, S.; Sehrawat, P.; Hashmi, S.A. Triglyme-Based Solvate Ionic Liquid Gelled in a Polymer: A Novel Electrolyte Composition for Sodium Ion Battery. *Mater. Today Commun.* **2022**, *31*, 103392. [CrossRef]
224. Goktas, M.; Akduman, B.; Huang, P.; Balducci, A.; Adelhelm, P. Temperature-Induced Activation of Graphite Co-Intercalation Reactions for Glymes and Crown Ethers in Sodium-Ion Batteries. *J. Phys. Chem. C* **2018**, *122*, 26816–26824. [CrossRef]
225. Murali, A.S.; Susan Baji, D.; Nair, S.; Santhanagopalan, D. Vapour Phase Conversion of Metal Oxalates to Metal Phosphide Nanostructures and Their Use as Anode in Rechargeable Li, Na and K-Ion Batteries. *Electrochim. Acta* **2021**, *388*, 138643. [CrossRef]
226. Wen, Y.; He, K.; Zhu, Y.; Han, F.; Xu, Y.; Matsuda, I.; Ishii, Y.; Cumings, J.; Wang, C. Expanded Graphite as Superior Anode for Sodium-Ion Batteries. *Nat. Commun.* **2014**, *5*, 4033. [CrossRef]
227. Ding, J.; Zhou, X.; Gao, J.; Lei, Z. Activating Graphite with Defects and Oxygenic Functional Groups to Boost Sodium-Ion Storage. *Nanoscale* **2023**, *15*, 13760–13769. [CrossRef]
228. Luo, P.; Zheng, C.; He, J.; Tu, X.; Sun, W.; Pan, H.; Zhou, Y.; Rui, X.; Zhang, B.; Huang, K. Structural Engineering in Graphite-Based Metal-Ion Batteries. *Adv. Funct. Mater.* **2022**, *32*, 2107277. [CrossRef]
229. Hu, M.; Zhou, H.; Gan, X.; Yang, L.; Huang, Z.-H.; Wang, D.-W.; Kang, F.; Lv, R. Ultrahigh Rate Sodium Ion Storage with Nitrogen-Doped Expanded Graphite Oxide in Ether-Based Electrolyte. *J. Mater. Chem. A* **2018**, *6*, 1582–1589. [CrossRef]
230. Liao, K.; Wang, H.; Wang, L.; Xu, D.; Wu, M.; Wang, R.; He, B.; Gong, Y.; Hu, X. A High-Energy Sodium-Ion Capacitor Enabled by a Nitrogen/Sulfur Co-Doped Hollow Carbon Nanofiber Anode and an Activated Carbon Cathode. *Nanoscale Adv.* **2019**, *1*, 746–756. [CrossRef]
231. Bommier, C.; Surta, T.W.; Dolgos, M.; Ji, X. New Mechanistic Insights on Na-Ion Storage in Nongraphitizable Carbon. *Nano Lett.* **2015**, *15*, 5888–5892. [CrossRef] [PubMed]
232. Zhong, B.; Liu, C.; Xiong, D.; Cai, J.; Li, J.; Li, D.; Cao, Z.; Song, B.; Deng, W.; Peng, H.; et al. Biomass-Derived Hard Carbon for Sodium-Ion Batteries: Basic Research and Industrial Application. *ACS Nano* **2024**, *18*, 16468–16488. [CrossRef] [PubMed]
233. Agrawal, A.; Janakiraman, S.; Biswas, K.; Venimadhav, A.; Srivastava, S.K.; Ghosh, S. Understanding the Improved Electrochemical Performance of Nitrogen-Doped Hard Carbons as an Anode for Sodium Ion Battery. *Electrochim. Acta* **2019**, *317*, 164–172. [CrossRef]
234. Jin, Q.; Wang, K.; Feng, P.; Zhang, Z.; Cheng, S.; Jiang, K. Surface-Dominated Storage of Heteroatoms-Doping Hard Carbon for Sodium-Ion Batteries. *Energy Storage Mater.* **2020**, *27*, 43–50. [CrossRef]
235. Doeff, M.M.; Ma, Y.; Visco, S.J.; De Jonghe, L.C. Electrochemical Insertion of Sodium into Carbon. *J. Electrochem. Soc.* **1993**, *140*, L169–L170. [CrossRef]
236. Luo, W.; Jian, Z.; Xing, Z.; Wang, W.; Bommier, C.; Lerner, M.M.; Ji, X. Electrochemically Expandable Soft Carbon as Anodes for Na-Ion Batteries. *ACS Cent. Sci.* **2015**, *1*, 516–522. [CrossRef]
237. Wan, X.; Li, Y.; Chen, S.; Duan, W.; Lei, W. Cathode Modification of Sodium-Ion Batteries for Improved Energy Density: A Review. *Adv. Sustain. Syst.* **2024**, *8*, 2400229. [CrossRef]
238. Bommier, C.; Luo, W.; Gao, W.-Y.; Greaney, A.; Ma, S.; Ji, X. Predicting Capacity of Hard Carbon Anodes in Sodium-Ion Batteries Using Porosity Measurements. *Carbon* **2014**, *76*, 165–174. [CrossRef]
239. Wang, K.; Sun, F.; Wang, H.; Wu, D.; Chao, Y.; Gao, J.; Zhao, G. Altering Thermal Transformation Pathway to Create Closed Pores in Coal-Derived Hard Carbon and Boosting of Na^+ Plateau Storage for High-Performance Sodium-Ion Battery and Sodium-Ion Capacitor. *Adv. Funct. Mater.* **2022**, *32*, 2203725. [CrossRef]
240. He, X.-X.; Zhao, J.-H.; Lai, W.-H.; Li, R.; Yang, Z.; Xu, C.; Dai, Y.; Gao, Y.; Liu, X.-H.; Li, L.; et al. Soft-Carbon-Coated, Free-Standing, Low-Defect, Hard-Carbon Anode To Achieve a 94% Initial Coulombic Efficiency for Sodium-Ion Batteries. *ACS Appl. Mater. Interfaces* **2021**, *13*, 44358–44368. [CrossRef]
241. Zhu, Y.; Chen, M.; Li, Q.; Yuan, C.; Wang, C. A Porous Biomass-Derived Anode for High-Performance Sodium-Ion Batteries. *Carbon* **2018**, *129*, 695–701. [CrossRef]
242. Zhao, Y.; Hu, Z.; Fan, C.; Gao, P.; Zhang, R.; Liu, Z.; Liu, J.; Liu, J. Novel Structural Design and Adsorption/Insertion Coordinating Quasi-Metallic Na Storage Mechanism toward High-Performance Hard Carbon Anode Derived from Carboxymethyl Cellulose. *Small* **2023**, *19*, 2303296. [CrossRef]

243. Meng, Q.; Lu, Y.; Ding, F.; Zhang, Q.; Chen, L.; Hu, Y.-S. Tuning the Closed Pore Structure of Hard Carbons with the Highest Na Storage Capacity. *ACS Energy Lett.* **2019**, *4*, 2608–2612. [CrossRef]
244. Fan, X.; Kong, X.; Zhang, P.; Wang, J. Research Progress on Hard Carbon Materials in Advanced Sodium-Ion Batteries. *Energy Storage Mater.* **2024**, *69*, 103386. [CrossRef]
245. Liu, G.; Ouyang, M.; Lu, L.; Li, J.; Han, X. Analysis of the Heat Generation of Lithium-Ion Battery During Charging and Discharging Considering Different Influencing Factors. *J. Therm. Anal. Calorim.* **2014**, *116*, 1001–1010. [CrossRef]
246. Liu, X.; Ren, D.; Hsu, H.; Feng, X.; Xu, G.-L.; Zhuang, M.; Gao, H.; Lu, L.; Han, X.; Chu, Z.; et al. Thermal Runaway of Lithium-Ion Batteries Without Internal Short Circuit. *Joule* **2018**, *2*, 2047–2064. [CrossRef]
247. Qi, C.; Wang, H.; Li, M.; Li, C.; Li, Y.; Shi, C.; Wei, N.; Wang, Y.; Zhang, H. Research on the Thermal Runaway Behavior and Flammability Limits of Sodium-Ion and Lithium-Ion Batteries. *Batteries* **2025**, *11*, 24. [CrossRef]
248. Zeng, G.; Liu, Y.; Gu, C.; Zhang, K.; An, Y.; Wei, C.; Feng, J.; Ni, J. A Nonflammable Fluorinated Carbonate Electrolyte for Sodium-Ion Batteries. *Acta Phys.-Chim. Sin.* **2020**, *36*, 1905006.
249. Zhao, X.; Zhuang, Q.-C.; Shi, Y.-L.; Zhang, X.-X. Influence of Vinylene Carbonate as an Additive on the Electrochemical Performances of Graphite Electrode in Poly(Methyl Methacrylate) Gel Polymer Electrolytes. *J. Appl. Electrochem.* **2015**, *45*, 1013–1023. [CrossRef]
250. Yang, Y.; Wu, C.; He, X.; Zhao, J.; Yang, Z.; Li, L.; Wu, X.; Li, L.; Chou, S. Boosting the Development of Hard Carbon for Sodium-Ion Batteries: Strategies to Optimize the Initial Coulombic Efficiency. *Adv. Funct. Mater.* **2024**, *34*, 2302277. [CrossRef]
251. Wen, Y.; Wang, B.; Zeng, G.; Nogita, K.; Ye, D.; Wang, L. Electrochemical and Structural Study of Layered P2-Type $\text{Na}_{2/3}\text{Ni}_{1/3}\text{Mn}_{2/3}\text{O}_2$ as Cathode Material for Sodium-Ion Battery. *Chem.-Asian J.* **2015**, *10*, 661–666. [CrossRef]
252. Deng, W.; Feng, X.; Xiao, Y.; Li, C. Layered Molybdenum (Oxy) Pyrophosphate $(\text{MoO}_2)_2\text{P}_2\text{O}_7$ as a Cathode Material for Sodium-Ion Batteries. *ChemElectroChem* **2018**, *5*, 1032–1036. [CrossRef]
253. Dang, R.; Chen, M.; Li, Q.; Wu, K.; Lee, Y.L.; Hu, Z.; Xiao, X. Na^+ -Conductive $\text{Na}_2\text{Ti}_3\text{O}_7$ -Modified P2-Type $\text{Na}_{2/3}\text{Ni}_{1/3}\text{Mn}_{2/3}\text{O}_2$ via a Smart In Situ Coating Approach: Suppressing Na^+ /Vacancy Ordering and P2–O2 Phase Transition. *ACS Appl. Mater. Interfaces* **2019**, *11*, 856–864. [CrossRef] [PubMed]
254. Kong, W.; Wang, H.; Sun, L.; Su, C.; Liu, X. Understanding the Synergic Roles of MgO Coating on the Cycling and Rate Performance of $\text{Na}_{0.67}\text{Mn}_{0.5}\text{Fe}_{0.5}\text{O}_2$ Cathode. *Appl. Surf. Sci.* **2019**, *497*, 143814. [CrossRef]
255. Jo, J.H.; Choi, J.U.; Konarov, A.; Yashiro, H.; Yuan, S.; Shi, L.; Sun, Y.; Myung, S. Sodium-Ion Batteries: Building Effective Layered Cathode Materials with Long-Term Cycling by Modifying the Surface via Sodium Phosphate. *Adv. Funct. Mater.* **2018**, *28*, 1705968. [CrossRef]
256. Sekine, S.; Hosaka, T.; Maejima, H.; Tatara, R.; Nakayama, M.; Komaba, S. $\text{Na}[\text{Mn}_{0.36}\text{Ni}_{0.44}\text{Ti}_{0.15}\text{Fe}_{0.05}] \text{O}_2$ Predicted via Machine Learning for High Energy Na-Ion Batteries. *J. Mater. Chem. A* **2024**, *12*, 31103–31107. [CrossRef]
257. Nekahi, A.; Dorri, M.; Rezaei, M.; Bouguern, M.D.; Madikere Raghunatha Reddy, A.K.; Li, X.; Deng, S.; Zaghib, K. Comparative Issues of Metal-Ion Batteries Toward Sustainable Energy Storage: Lithium vs. Sodium. *Batteries* **2024**, *10*, 279. [CrossRef]
258. Hirsh, H.S.; Li, Y.; Tan, D.H.S.; Zhang, M.; Zhao, E.; Meng, Y.S. Sodium-Ion Batteries Paving the Way for Grid Energy Storage. *Adv. Energy Mater.* **2020**, *10*, 2001274. [CrossRef]
259. IEA. *Global EV Outlook 2023*; International Energy Agency (IEA): Paris, France, 2023.
260. Environmental Impacts of Lithium-Ion Batteries. Available online: <https://www.instituteforenergyresearch.org/renewable/environmental-impacts-of-lithium-ion-batteries/> (accessed on 20 February 2025).
261. Lilley, S. Sodium-ion Batteries: Inexpensive and Sustainable Energy Storage. *Faraday Insights* **2021**, *11*, 1–6. Available online: https://www.faraday.ac.uk/wp-content/uploads/2021/06/Faraday_Insights_11_FINAL.pdf (accessed on 20 February 2025).
262. Islam, M.T.; Iyer-Raniga, U. Lithium-Ion Battery Recycling in the Circular Economy: A Review. *Recycling* **2022**, *7*, 33. [CrossRef]
263. Subburam, G.; Ramachandran, K.; El-Khodary, S.A.; Zou, B.; Wang, J.; Wang, L.; Qiu, J.; Liu, X.; Ng, D.H.L.; Lian, J. Development of Porous Carbon Nanosheets from Polyvinyl Alcohol for Sodium-Ion Capacitors. *Chem. Eng. J.* **2021**, *415*, 129012. [CrossRef]
264. Xiao, L.; Lu, H.; Fang, Y.; Sushko, M.L.; Cao, Y.; Ai, X.; Yang, H.; Liu, J. Low-Defect and Low-Porosity Hard Carbon with High Coulombic Efficiency and High Capacity for Practical Sodium Ion Battery Anode. *Adv. Energy Mater.* **2018**, *8*, 1703238. [CrossRef]
265. Zhang, X.; Yang, J.; Ren, Z.; Xie, K.; Ye, Q.; Xu, F.; Liu, X. In-Situ Observation of Electrolyte-Dependent Interfacial Change of the Graphite Anode in Sodium-Ion Batteries by Atomic Force Microscopy. *New Carbon Mater.* **2022**, *37*, 371–379. [CrossRef]
266. Pendashteh, A.; Orayech, B.; Suhard, H.; Jauregui, M.; Ajuria, J.; Silván, B.; Clarke, S.; Bonilla, F.; Saurel, D. Boosting the Performance of Soft Carbon Negative Electrode for High Power Na-Ion Batteries and Li-Ion Capacitors through a Rational Strategy of Structural and Morphological Manipulation. *Energy Storage Mater.* **2022**, *46*, 417–430. [CrossRef]
267. Liu, K.; Liu, W.; Qiu, Y.; Kong, B.; Sun, Y.; Chen, Z.; Zhuo, D.; Lin, D.; Cui, Y. Electrospun Core-Shell Microfiber Separator with Thermal-Triggered Flame-Retardant Properties for Lithium-Ion Batteries. *Sci. Adv.* **2017**, *3*, e1601978. [CrossRef] [PubMed]
268. Jian, Z.; Bommier, C.; Luo, L.; Li, Z.; Wang, W.; Wang, C.; Greaney, P.A.; Ji, X. Insights on the Mechanism of Na-Ion Storage in Soft Carbon Anode. *Chem. Mater.* **2017**, *29*, 2314–2320. [CrossRef]
269. Evarts, E.C. Lithium Batteries: To the Limits of Lithium. *Nature* **2015**, *526*, S93–S95. [CrossRef]

270. Jia, H.; Zou, L.; Gao, P.; Cao, X.; Zhao, W.; He, Y.; Engelhard, M.H.; Burton, S.D.; Wang, H.; Ren, X.; et al. High-Performance Silicon Anodes Enabled by Nonflammable Localized High-Concentration Electrolytes. *Adv. Energy Mater.* **2019**, *9*, 1900784. [[CrossRef](#)]
271. Kubota, K.; Dahbi, M.; Hosaka, T.; Kumakura, S.; Komaba, S. Towards K-Ion and Na-Ion Batteries as “Beyond Li-Ion”. *Chem. Rec.* **2018**, *18*, 459–479. [[CrossRef](#)]
272. Lewis, G.N.; Keyes, F.G. The potential of the lithium electrode. *J. Am. Chem. Soc.* **1913**, *35*, 340–344. [[CrossRef](#)]
273. Li, Q.; Jiao, S.; Luo, L.; Ding, M.S.; Zheng, J.; Cartmell, S.S.; Wang, C.-M.; Xu, K.; Zhang, J.-G.; Xu, W. Wide-Temperature Electrolytes for Lithium-Ion Batteries. *ACS Appl. Mater. Interfaces* **2017**, *9*, 18826–18835. [[CrossRef](#)] [[PubMed](#)]
274. Newman, G.H.; Klemann, L.P. Ambient Temperature Cycling of an Na-TiS₂ Cell. *J. Electrochem. Soc.* **1980**, *127*, 2097–2099. [[CrossRef](#)]
275. Paolella, A.; Faure, C.; Bertoni, G.; Marras, S.; Guerfi, A.; Darwiche, A.; Hovington, P.; Commarie, B.; Wang, Z.; Prato, M.; et al. Light-Assisted Delithiation of Lithium Iron Phosphate Nanocrystals towards Photo-Rechargeable Lithium Ion Batteries. *Nat. Commun.* **2017**, *8*, 14643. [[CrossRef](#)]
276. Rudola, A.; Rennie, A.J.R.; Heap, R.; Meysami, S.S.; Lowbridge, A.; Mazzali, F.; Sayers, R.; Wright, C.J.; Barker, J. Commercialisation of High Energy Density Sodium-Ion Batteries: Faradion’s Journey and Outlook. *J. Mater. Chem. A* **2021**, *9*, 8279–8302. [[CrossRef](#)]
277. Sayahpour, B.; Hirsh, H.; Parab, S.; Nguyen, L.H.B.; Zhang, M.; Meng, Y.S. Perspective: Design of Cathode Materials for Sustainable Sodium-Ion Batteries. *MRS Energy Sustain.* **2022**, *9*, 183–197. [[CrossRef](#)]
278. Song, L.; Li, S.; Wang, J.; Zhu, J.; Wang, Y.; Cai, X.; Zong, F.; Wang, H.; Cui, X.; Zhao, D. Building a Flexible and Highly Ionic Conductive Solid Electrolyte Interphase on the Surface of Si@C Anodes by Binary Electrolyte Additives. *ACS Appl. Mater. Interfaces* **2023**, *15*, 49727–49738. [[CrossRef](#)] [[PubMed](#)]
279. Wentker, M.; Greenwood, M.; Leker, J. A Bottom-Up Approach to Lithium-Ion Battery Cost Modeling with a Focus on Cathode Active Materials. *Energies* **2019**, *12*, 504. [[CrossRef](#)]
280. Whittingham, M.S. Electrical Energy Storage and Intercalation Chemistry. *Science* **1976**, *192*, 1126–1127. [[CrossRef](#)]
281. Winter, M. The Solid Electrolyte Interphase—The Most Important and the Least Understood Solid Electrolyte in Rechargeable Li Batteries. *Z. Für Phys. Chem.* **2009**, *223*, 1395–1406. [[CrossRef](#)]
282. Yabuuchi, N.; Hara, R.; Kubota, K.; Paulsen, J.; Kumakura, S.; Komaba, S. A New Electrode Material for Rechargeable Sodium Batteries: P2-Type Na_{2/3}[Mg_{0.28}Mn_{0.72}]O₂ with Anomalously High Reversible Capacity. *J. Mater. Chem. A* **2014**, *2*, 16851–16855. [[CrossRef](#)]
283. Yabuuchi, N.; Kajiyama, M.; Iwatate, J.; Nishikawa, H.; Hitomi, S.; Okuyama, R.; Usui, R.; Yamada, Y.; Komaba, S. P2-Type Na_x[Fe_{1/2}Mn_{1/2}]O₂ Made from Earth-Abundant Elements for Rechargeable Na Batteries. *Nat. Mater.* **2012**, *11*, 512–517. [[CrossRef](#)] [[PubMed](#)]
284. CATL: CATL Unveils Its Latest Breakthrough Technology by Releasing Its First Generation of Sodium-Ion Batteries. Available online: <https://www.catl.com/en/news/665.html> (accessed on 29 July 2021).

Disclaimer/Publisher’s Note: The statements, opinions and data contained in all publications are solely those of the individual author(s) and contributor(s) and not of MDPI and/or the editor(s). MDPI and/or the editor(s) disclaim responsibility for any injury to people or property resulting from any ideas, methods, instructions or products referred to in the content.